Ore Geology Reviews 90 (2017) 618–633

Contents lists available at ScienceDirect

Ore Geology Reviews

journal homepage: www.elsevier.com/locate/oregeorev

Geochronological and geochemical constraints on sulfide mineralization in the Qingmingshan mafic intrusion in the western part of the Proterozoic Jiangnan orogenic belt along the southern margin of the Yangtze Craton

Yi Zhou[a,b], Hong Zhong[a,*], Chusi Li[c], Edward M. Ripley[c], Wei-Guang Zhu[a], Zhong-Jie Bai[a], Chao Li[d]

[a] State Key Laboratory of Ore Deposit Geochemistry, Institute of Geochemistry, Chinese Academy of Sciences, Guiyang 550081, China
[b] University of Chinese Academy of Sciences, Beijing 100049, China
[c] Department of Earth and Atmospheric Sciences, Indiana University, Bloomington, IN 47405, USA
[d] National Research Center for Geoanalysis, Beijing 100037, China

ARTICLE INFO

Keywords:
Zircon U-Pb age
Os-S isotopes
Sulfide mineralization
PGE geochemistry
Mafic-ultramafic rocks
Jiangnan orogenic belt
South China

ABSTRACT

The Qingmingshan magmatic Fe-Ni-Cu sulfide deposit is located in the southern margin of the Yangtze Craton, in the western part of the Proterozoic Jiangnan orogenic belt. Sulfide mineralization occurs as disseminated zones in a dike-like mafic body intruding Early Neoproterozoic meta-sedimentary rocks. The host intrusion can be further divided into an upper gabbronorite unit, a middle dolerite unit and a lower gabbronorite unit. Each unit contains at least one disseminated sulfide zone. Sulfide mineral assemblages are composed of pyrrhotite, pentlandite and chalcopyrite. Zircon U–Pb dating yields a crystallization age of 847.8 ± 3.8 Ma (2σ) for the intrusion. The host rocks are characterized by enrichment in light rare earth elements (REE) relative to heavy REE and show pronounced negative Nb-Ta anomalies, similar to the characteristics of arc mafic igneous rocks worldwide. Mixing calculations indicate that the variations of $(Th/Yb)_N$ and $(Th/Nb)_N$ in the intrusion are consistent with between 10 and 20 wt% crustal contamination of the parental magma. The sulfide separates are characterized by elevated $\delta^{34}S$ values from 1.5 to 3.5‰, with a peak at 2.6‰, and by γ_{Os} values from 2 to 89, indicating addition of crustal sulfur and Os to the parental magma. The trace element data and S-Os isotopes support the premise that sulfide saturation in the Qingmingshan magma was triggered by crustal contamination. Variations of PGE tenors in different sulfide zones can be explained by variable R-factors from 300 to 1000 during sulfide segregation from the magma. Mass balance calculations indicate that the parental magma was severely depleted in PGE, which could be a primary signature of arc basaltic magma formed by low degrees of partial melting or due to previous sulfide segregation at depth. The lithological and mineralization zonation across the dike-like Qingmingshan mafic intrusion indicates that at least three separate pulses of sulfide-charged magma were involved in the formation of the Qingmingshan magmatic sulfide deposit. The Qingmingshan mafic intrusion is interpreted to be a part of a sub-arc magma plumbing system. Coeval ultramafic intrusions formed from more primitive magma in the region are good exploration targets for magmatic sulfide deposits with higher Ni/Cu ratios than the Qingmingshan deposit.

1. Introduction

The Qingmingshan Fe-Ni-Cu sulfide deposit occurs in the Baotan region that is part of the Yangtze Craton. It is one of several known magmatic sulfide deposits that formed in the Neoproterozoic in China (Fig. 1a), such as the Lengshuiqing deposit in the western rim of the Yangtze Craton (817 ± 5 Ma; Munteanu et al., 2010), the Xingdi deposit in the northern rim of the Tarim Craton (737 ± 2 Ma; Han et al., 2016), and the giant Jinchuan deposit in the southwestern rim of the North China Craton (831.8 ± 0.6 Ma; Zhang et al., 2010). Owing to its super-large size, the Jinchuan deposit has been studied most extensively and is thus well known to the world. In contrast, little is known about the genetic controls on the Qingmingshan deposit. In fact, this deposit has never been reported in any international journal. However, a better understanding of this deposit, especially its age and the lithological control on sulfide mineralization, can be used to assist the on-going regional Ni exploration. The greater Baotan region has been selected by the China Geological Survey as a nickel exploration

* Corresponding author.
E-mail address: zhonghong@vip.gyig.ac.cn (H. Zhong).

http://dx.doi.org/10.1016/j.oregeorev.2017.08.031
Received 4 December 2016; Received in revised form 10 August 2017; Accepted 17 August 2017
Available online 24 August 2017

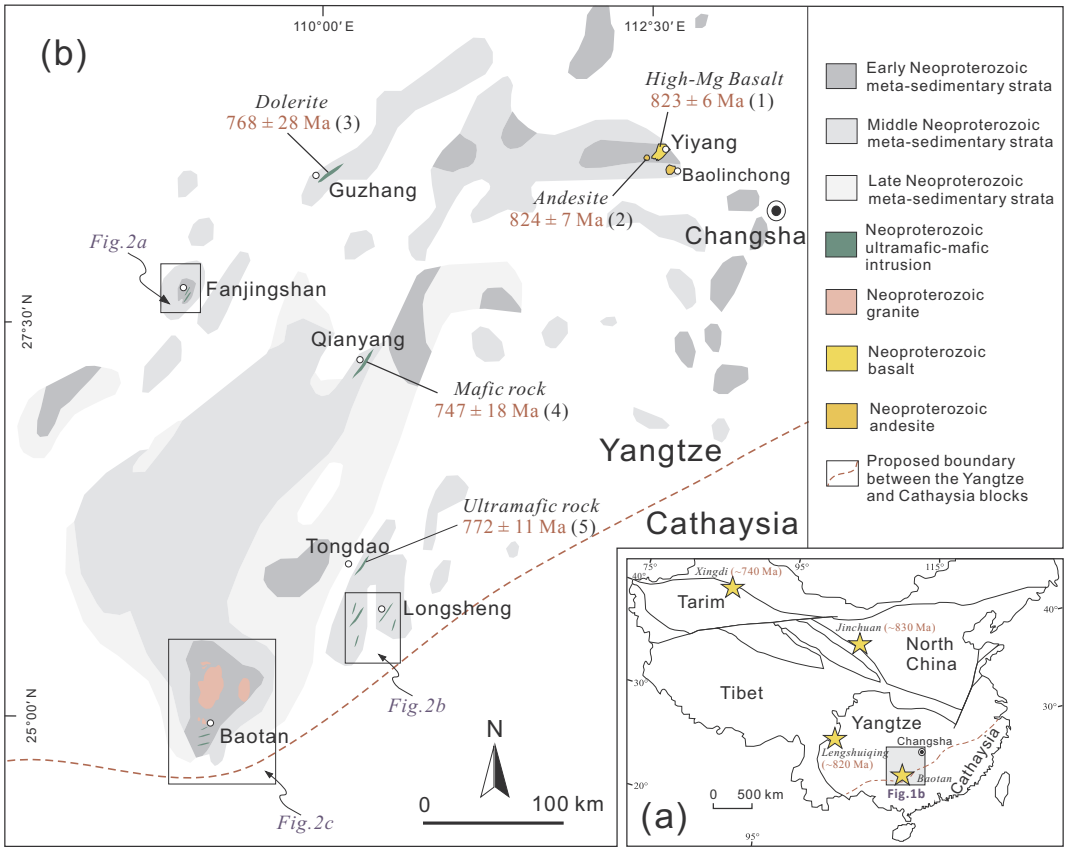

Fig. 1. (a) The tectonic units of China (modified from Zhao and Cawood, 2012), showing the location of the Neoproterozoic Jinchuan, Lengshuiqing and Xingdi magmatic sulfide deposits with ages, (b) Simplified geological map of the western Jiangnan orogenic belt in the southern margin of the Yangtze Craton (modified from Zhao, 2015), showing the distribution of the representative Neoproterozoic igneous rocks with different ages. The age data are from Table 1.

target mainly because there are many Neoproterozoic mafic-ultramafic intrusions in the region, including the host of the Qingmingshan magmatic Fe-Ni-Cu sulfide deposit.

The tectonic setting of the Qingmingshan magmatic sulfide deposit is controversial. Some researchers (e.g., Li et al., 2005) suggested that the Qingmingshan magmatic sulfide deposit in the southern rim of the Yangtze Craton and the giant Jinchuan magmatic Fe-Ni-Cu sulfide deposit in the southwestern rim of the North China Craton (see Fig. 1a for locations) are linked to the same Neoproterozoic mantle plume before the break up of Rodinia. Other researchers (e.g., Zhou et al., 2004; Wang et al., 2008; Zhao and Zhou, 2013) argued that the mafic-ultramafic rocks including the host of the Qingmingshan magmatic sulfide deposit in the southern rim of the Yangtze Craton are the products of arc basaltic magmatism in the Neoproterozoic. Clearly, a detailed petrological study of the Qingmingshan deposit can shed new lights on the debate.

Mao and Du (2002) reported a Re-Os isochron age of 982 ± 21 using samples from some sulfide occurrences in the Baotan area. Liu et al. (2010) and Yang et al. (2010a,b) reported in Chinese the major and trace element compositions for a limited number of samples from the Qingmingshan magmatic sulfide deposit as well as other sulfide occurrences in the area. This study reports a new zircon U-Pb age for the host intrusion of the Qingmingshan magmatic Fe-Ni-Cu sulfide deposit, plus integrated major, trace and platinum group element compositions, and Os-S isotopes for the deposit. The zircon U-Pb age is used to establish a reliable temporal relationship between regional basaltic magmatism and sulfide mineralization while the geochemical data are used to evaluate the lithological control on sulfide mineralization as well as the cause of sulfide saturation in the magma. The implications of our new results for regional tectonomagmatism and Ni exploration are also discussed.

2. Geological background

The South China Block comprises the Yangtze Craton to the north and the Cathaysia Block to the south. The Proterozoic Jiangnan orogenic belt in the southern margin of the Yangtze Craton is widely interpreted to be a northwest-oriented subduction-collision zone between the Yangtze and Cathaysia Blocks (e.g., Zhao and Cawood, 1999; Li et al., 2002; Zhou et al., 2002).

The Jiangnan orogenic belt is mainly composed of Neoproterozoic igneous and sedimentary sequences and experienced ductile shearing and regional greenschist-facies to amphibolite-facies metamorphism during the assembly of the Yangtze and Cathaysia Blocks (Shu, 2012; Charvet, 2013). The Neoproterozoic strata in the Jiangnan orogenic belt consist of three distinct units (as shown in Fig. 1b) that are in unconformable contact (BGMRGX, 1985). The lower unconformity between the early-Neoproterozoic and middle-Neoproterozoic sequences corresponds to the Neoproterozoic Jiangnan orogeny (also termed as the ‘Sibao orogeny’ or the ‘Jinning orogeny’) in South China (Wang and Li, 2003; Wang et al., 2007), whereas the upper unconformity between the middle-Neoproterozoic and late-Neoproterozoic is thought to be correlated to the breakup of the South China Block (Wang and Li, 2003).

The early-Neoproterozoic sequences, known as the Sibao Group in northern Guangxi, constitute the Neoproterozoic basement of the western Jiangnan orogen. The Sibao Group, with a thickness over 5700 m, consists dominantly of low-grade metamorphosed bathyal-abyssal terrigenous clastic rocks, such as sandstone, siltstone and mudstone, with interlayers of volcanic rocks (Figs. 1b and 2) (BGMRGX, 1985). The Sibao Group is overlain unconformably by the middle-Neoproterozoic strata (known as the Danzhou Group in northern Guangxi) and the late-Neoproterozoic (Sinian) cover. Detrital zircon age data and stratigraphic correlation indicate that the Sibao Group was

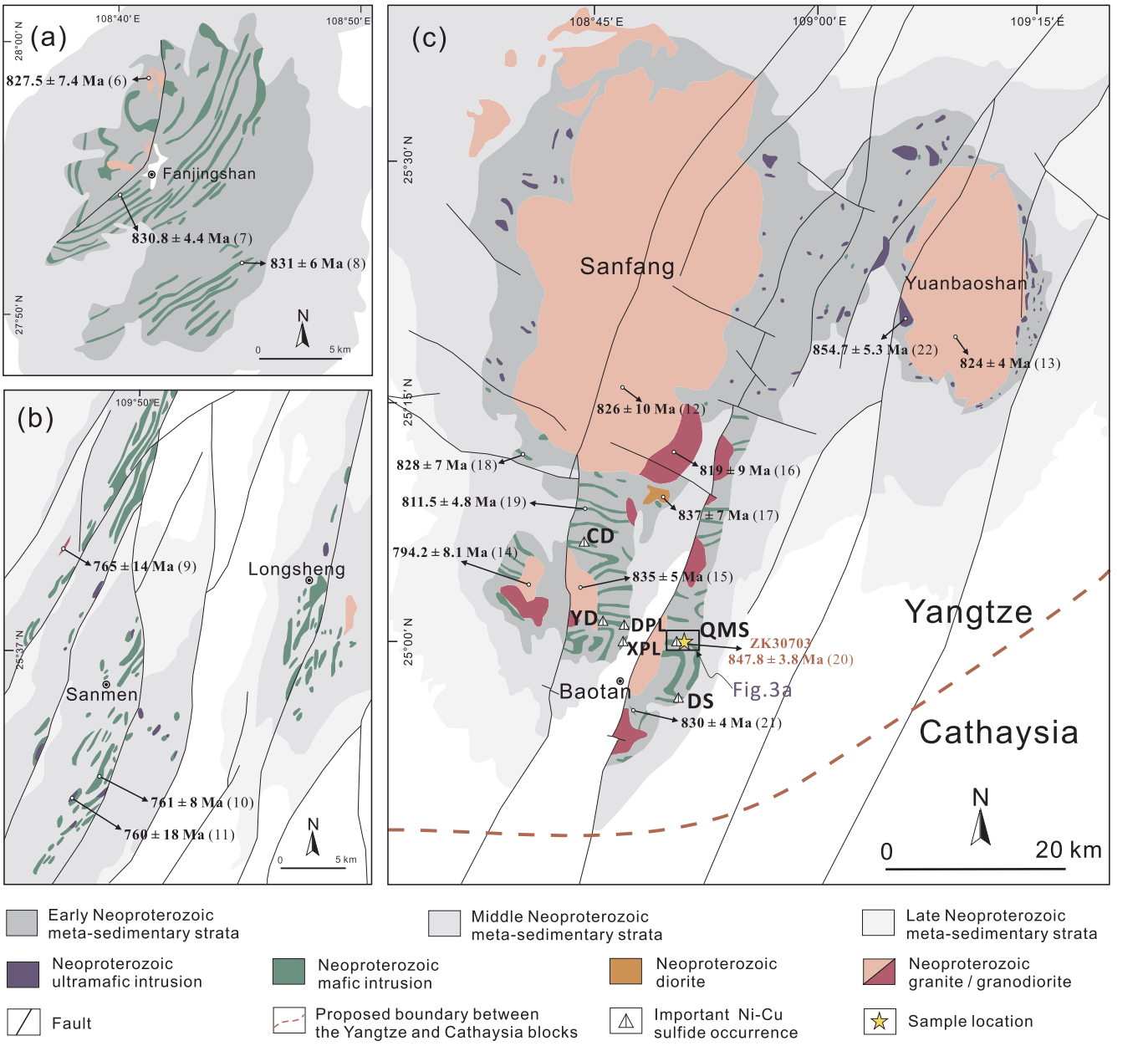

Fig. 2. Simplified geological maps showing a cluster of mafic-ultramafic intrusions and granitoids with different ages: (a) Fanjingshan area (modified after GZRGST, 1974; BGMRGZ, 1987), (b) Sanmen-Longsheng area (modified after GXRGST, 1964; GXRGST, 1966), (c) Baotan area (modified after GXRGST, 1987, 1995). See Table 1 and associated text for details of age data, and see Table 2 for Ni-Cu occurrences in the Baotan area. QMS = Qingmingshan deposit, YD = Yidong deposit, DPL = Dapoling deposit, XPL = Xiaopoling deposit, DS = Disu deposit, CD = Chidong deposit.

deposited between 870 and 830 Ma (Zhao et al., 2011; Wang et al., 2007, 2012 and references therein).

Neoproterozoic (mainly between 850 and 740 Ma) mafic to granitic magmatism (mainly between 840 and 800 Ma) are widespread in the western segment of the Jiangnan orogenic belt (Fig. 1b, 2 and Table 1). There are more than 300 outcrops of mafic-ultramafic rocks in the region (BGMRGX, 1985; Wang et al., 2006), some of which are in turn truncated by granitic plutons.

Li et al. (1999) reported a U-Pb zircon age of 828 ± 7 Ma from several mafic-ultramafic dikes intruding the Sibao Group in northern Guangxi (Fig. 2c). These dikes were interpreted by the authors to be the products of the "South China Mantle Plume". In contrast, slightly older mafic-ultramafic rocks with zircon U-Pb ages of ~850 Ma in the region were thought to be subduction-related (Yao et al., 2014). Zhao and Zhou (2013) reported the occurrence of ~830 Ma boninitic lavas within the Sibao Group in the region and regarded these lavas as evidence for an arc setting for Neoproterozoic. A mafic intrusion of 830 ± 4 Ma is present in the vicinity of Baotan (Wang et al., 2012). A dolerite dike of 811.5 ± 4.8 Ma is present in the nearby Hejiawan area (Wang et al., 2006). High-Mg diorite plutons thought to be subduction-related, such as the Dongma pluton with a zircon U-Pb age of 837 ± 7 Ma, are common in the region (Wang et al., 2014; Chen et al., 2014). The granitoids in the region mainly belong to the S-type and formed between 840 and 800 Ma (Li, 1999; Wang et al., 2006, 2014).

About 16 Fe-Ni-Cu sulfide occurrences associated with mafic-ultramafic rocks have been reported for the Baotan region (Fig. 2c and Table 2). The most important ones are the Qingmingshan, Dapoling-Yidong, Xiaopoling and Disu occurrences. An on-going exploration campaign has delineated ~24000 metric tons of Ni, ~13000 metric tons of Cu, with the average grades of 0.25 wt% for Ni and 0.13 wt% for Cu, in the Qingmingshan deposit (personal communication with an exploration geologist in charge, July 2017).

Table 1
A compilation of representative zircon U-Pb ages for the Neoproterozoic igneous rocks in the southwest Yangtze Craton.

No.	Rock type	Locality	Age (Ma)	Method	Reference
Fig.1(b)					
(1)	High-Mg basalt	Yiyang, Northern Hunan	823 ± 6	SHRIMP	Wang et al. (2007)
(2)	Tuffaceous andesite	Baiyangzhuang, Yiyang, Northern Hunan	824 ± 7	SIMS	Zhang et al. (2012)
(3)	Dolerite	Guzhang, Western Hunan	768 ± 28	SHRIMP	Zhou et al. (2007)
(4)	Mafic rock	Qianyang, Western Hunan	747 ± 18	SHRIMP	Wang et al. (2008)
(5)	Ultramafic rock	Tongdao, Western Hunan	772 ± 11	SHRIMP	Wang et al. (2008)
Fig.2(a) Fanjingshan area					
(6)	Leucogranite	Fanjingshan, Eastern Guizhou	827.5 ± 7.4	SIMS	Zhao et al. (2011)
(7)	Volcanic rock	Fanjingshan, Eastern Guizhou	830.8 ± 4.4	SIMS	Zhao et al. (2011)
(8)	Dolerite	Fanjingshan, Eastern Guizhou	831 ± 6	La-ICPMS	Zhou et al. (2009)
Fig.2(b) Sanmenjie-Longsheng area					
(9)	Rhyodacite	Sanmenjie, Northern Guangxi	765 ± 14	SHRIMP	Zhou et al. (2007)
(10)	Gabbro-diabase	Sanmenjie, Northern Guangxi	761 ± 8	TIMS	Ge et al. (2001)
(11)	Serpentinite	Sanmenjie, Northern Guangxi	760 ± 18	La-ICPMS	Lin et al. (2016)
Fig.2(c) Baotan area					
(12)	Biotite granite	Sanfang, Northern Guangxi	826 ± 10	SHRIMP, TIMS	Li et al. (1999)
(13)	Biotite granite	Yuanbaoshan, Northern Guangxi	824 ± 4	SHRIMP, TIMS	Li et al. (1999)
(14)	Biotite granite	Tianpeng, Northern Guangxi	794.2 ± 8.1	La-ICPMS	Wang et al. (2006)
(15)	Biotite granite	Pingying, Northern Guangxi	835 ± 5	La-ICPMS	Wang et al. (2014)
(16)	Granodiorite	Bendong, Northern Guangxi	819 ± 9	SHRIMP, TIMS	Li et al. (1999)
(17)	Diorite	Dongma, Northern Guangxi	837 ± 7	La-ICPMS	Wang et al. (2014), Chen et al. (2014)
(18)	Mafic rock	Yangmeiao, Northern Guangxi	828 ± 7	SHRIMP	Li et al. (1999)
(19)	Dolerite	Hejiawan, Northern Guangxi	811.5 ± 4.8	La-ICPMS	Wang et al. (2006)
(20)	Sulfide-bearing mafic rock	QMS occurrence, Northern Guangxi	847.8 ± 3.8	SIMS	This study
(21)	Mafic rock	Near Baotan, Northern Guangxi	830 ± 4	La-ICPMS	Wang et al. (2012)
(22)	Mafic-ultramafic rock	Yuanbaoshan, Northern Guangxi	854.7 ± 5.3	La-ICPMS	Yao et al. (2014)

Table 2
Occurrences of sulfide mineralization in mafic-ultramafic intrusions in the Baotan region.

Occurrence No.	Name of host intrusion	Intrusion geometry	Grades (wt.%)	
			Ni	Cu
1	Qingmingshan	Dike-like	0.20–0.47	0.10–0.24
2	Xiaopoling	Dike-like	0.21–0.33	0.10–0.15
3	Dapoling – Yidong	Dike-like	0.22–0.56	0.13–0.35
4	Disu	Dike-like	0.30–0.47	0.19–0.23
5	Chidong	Dike-like	0.21–0.52	0.15–0.30
6	Jiuhuangdashan	Dike-like	0.24–0.41	0.12–0.58
7	Honggangshan	Dike-like	0.31–0.45	0.05–0.27
8	Tianbian	Dike-like	0.11–0.29	0.10–0.26
9	Donglongshan	Dike-like	0.27–0.45	0.26–0.58
10	Yudoushan	Dike-like	0.22–2.10	0.17–0.90
11	Taojia	Dike-like	0.30–0.49	0.2 1–0.32
12	Macaoshan	Dike-like	0.20–0.30	0.10–0.30
13	Mandong	Dike-like	0.28–0.47	0.19–0.65
14	Xianrendong	Dike-like	0.43–0.46	0.28–0.30
15	Shanniuling	Dike-like	unknown	unknown
16	Wende	Dike-like	unknown	unknown

Data for the Qingmingshan deposit are unpublished data from the Jishengyuan Mining Ltd. Other data are from Yang et al. (2010a) and references therein.

3. Lithology and petrography

The Qingmingshan sulfide-bearing mafic intrusion is one of several subparallel south-dipping dike-like bodies intruding meta-pelitic siltstone, mudstone and sandstone that are interbedded with intermediate-mafic volcanic rocks (Fig. 3a and b). Important sulfide mineralization is present only in the Qingmingshan mafic intrusion but not in the nearby mafic intrusions. The thickness of the Qingmingshan mafic intrusion varies between 20 m and 60 m (Fig. 3b). The downward extension is unknown. Horizontal underground exploration tunnels in the upper portion of the dike down to ~200 m from the outcrop reveal two subparallel disseminated sulfide zones close to the upper contact with country rock (Fig. 3b). Drilling (ZK 1202) through the lower portion of the dike at ~600 m from the outcrop reveals three subparallel disseminated sulfide zones that are roughly evenly distributed across the dike (Fig. 3b). Drilling in between (CK 17) did not intercept any sulfide zones (Fig. 3b). The thicknesses of the disseminated sulfide zones vary from less than a half meter to several meters. In the upper part of the dike small massive sulfide veins (Fig. 4a) and irregular chalcopyrite-rich sulfide patches with quartz and calcite intergrowths (Fig. 4b, c) are present in places close to the disseminated sulfide zones. The disseminated sulfide zones are mainly composed of pyrrhotite, pentlandite and chalcopyrite, often present as the interstitial minerals between silicate minerals (Fig. 4d). Primary pyroxenes and plagioclase in the host rocks have been replaced by secondary amphiboles (Fig. 4e) and clinozoisite plus albite (Fig. 4f), respectively. According to the relict texture and norm composition calculation, the hosting rocks of the sulfides in the Qingmingshan deposit are mainly composed of cumulate gabbronorites, plus a dolerite with a characteristic poikilitic texture (Fig. 4f)

4. Sampling and analytical methods

A total of 29 samples were collected from the Qingmingshan sulfide-bearing mafic intrusion. Among them a large sample for age study was collected from drill core ZK30703, 22 samples were collected from drill cores ZK1202 and 6 samples were collected from two underground horizontal tunnels (Fig. 3b). Polished thin sections of the samples were used for petrographic study (Fig. 4c–f). 200 mesh powders of the samples prepared using an agate mill were used for chemical analysis.

The sample from drill core ZK30703 is an altered gabbronorite. Zircon grains were separated from this sample using conventional density and magnetic separation techniques. Together with the Plesovice and Qinghu zircon standards, the zircon grains from our sample were mounted in an epoxy resin, which was then polished for target selection and U-Pb analysis. Cathodoluminescence images were used to select un-deformed zircon crystals that show simple zoning or no zoning plus lack of inherited cores for U-Pb dating. U-Pb isotopes of the selected zircon crystals were determined using a CAMECA IMS-1280 SIMS at the Institute of Geology and Geophysics, Chinese Academy of Sciences, following the procedures of Li et al. (2009). Data

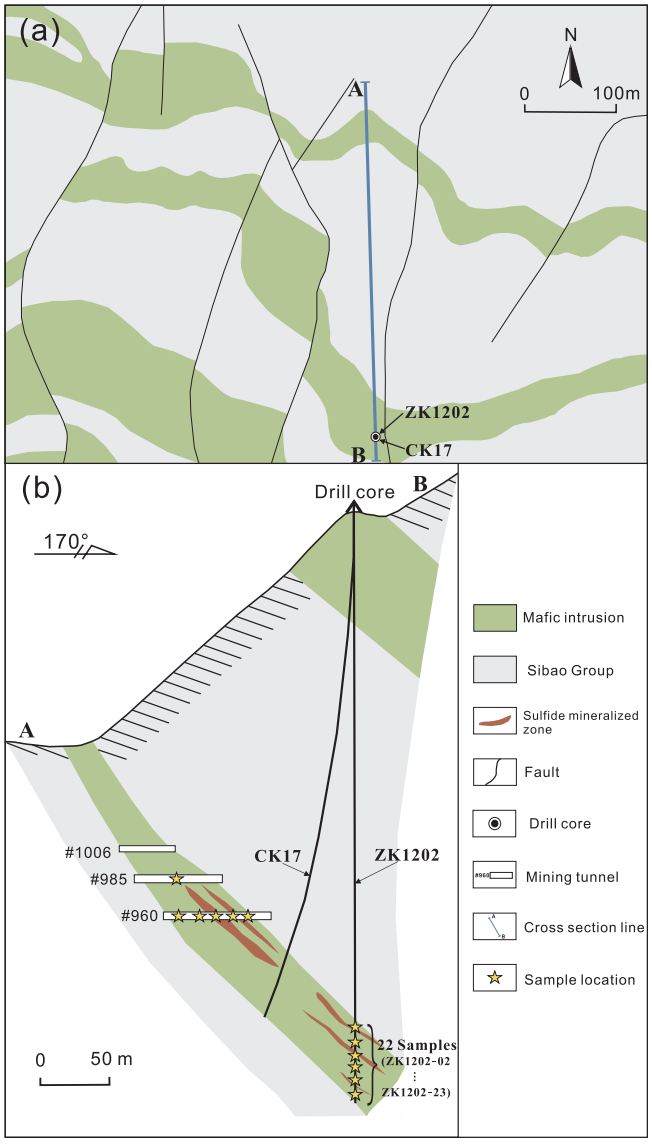

Fig. 3. (a) Sketch map of the QMS deposit with the location of the drill cores, (b) Cross section of the QMS deposit with the location of drill cores, mining tunnel and samples. Both figures are drawn based on unpublished data from the Jishengyuan Mining Ltd.

reduction was carried out using the ISOPLOT program of Ludwig (2012).

The abundances of major elements plus Cu and Ni in whole rocks were determined using X-ray fluorescence spectrometry in the ALS Laboratory in Guangzhou, China. The analytical uncertainty was estimated to be better than 5%. The contents of sulfur in whole rocks were determined using an infrared carbon-sulfur analyzer in the ALS Laboratory in Guangzhou, China. The concentrations of trace elements in whole rocks were determined using a Perkin-Elmer Sciex ELAN DRC-e ICP-MS in the State Key Laboratory of Ore Deposit Geochemistry (SKLODG), Institute of Geochemistry, Chinese Academy of Sciences, Guiyang, China. The powdered samples (50 mg) were dissolved in high-pressure Teflon bombs using HF + HNO_3 mixture for 48 h at ~190 °C (Qi et al., 2000). Rh was used as an internal standard to monitor signal drift during counting. The analytical uncertainty was estimated to be between 5% and 10%, depending on concentrations.

The concentrations of platinum-group elements (PGE) in sulfide-bearing rock samples were determined by acid digestion and isotope dilution (ID)-ICP-MS using a Perkin-Elmer Sciex ELAN DRC-e in the SKLODG, Institute of Geochemistry, Chinese Academy of Sciences, Guiyang, China. The sample preparation and analytical procedures are the same as given in Qi et al. (2011). The mono-isotopic element Rh was measured by external calibration using a ^{194}Pt spike as internal standard. About eight grams of rock powder were first digested by HF in a custom made 120 ml PTFE beaker on a hot plate to remove silicates. After that, the dried residue with an appropriate amount of enriched isotope spike solution containing ^{193}Ir, ^{101}Ru, ^{194}Pt and ^{105}Pd was digested with HF + HNO_3 at 190 °C for about 48 h after the beaker was sealed in a stainless steel pressure bomb. The total procedural blanks were lower than 0.002 ppb for Ir and Rh, 0.015 ppb for Ru, 0.002 ppb for Pt, and 0.04 ppb for Pd. The analytical error is within 10% of the accepted values, based on the results from the international standards (WGB-1 and WPR-1) analyzed together with our samples.

Re-Os isotopes of the selected sulfide-bearing samples were determined in the National Research Center for Geoanalysis, Chinese Academy of Geological Sciences in Beijing, China. The chemical separation procedure is the same as described in Li et al. (2015b and references therein). Enriched ^{190}Os and enriched ^{185}Re from the Oak Ridge National Laboratory were used. The purified Os and Re extracted from the samples were loaded to Pt filaments separately, and analyzed for isotope ratios using negative ion thermal ionization mass spectrometry. The measured Re and Os isotopic ratios were corrected for isobaric oxygen interferences, and mass fractionation using ^{185}Re/^{187}Re = 0.59738, and ^{192}Os/^{188}Os = 3.08271. The total procedural blanks were about 1.8 pg for Re, 0.26 pg for Os and 0.012 pg for ^{187}Os. The internal standard JCBY (the Jinchuan disseminated sulfide ore) was used to monitor accuracy. The Re and Os contents and ^{187}Os/^{188}Os ratio of the JCBY standard determined during the course of this work are 38.77 ± 0.11 ppb, 15.64 ± 0.05 ppb, and 0.336 ± 0.0006, respectively, which are similar to the certified values.

Sulfur isotope analysis was carried out at Indiana University, USA using the continuous-flow method described in Studley et al. (2002). Sulfide minerals such as pentlandite, chalcopyrite, and pyrrhotite were drilled from hand specimens using a 0.75-mm carbide bit. Sulfide powder ranging from 0.15 to 0.17 mg was placed in tin cups with approximately 1.5 to 2 mg vanadium pentoxide (V_2O_5). Samples were prepared in an elemental analyzer by flash combustion at 1800 °C with a reactor column temperature of 1010 °C. Measurements of produced SO_2 were made using a Finnigan Delta V stable isotope ratio mass spectrometer, with results reported in standard delta notation ($\delta^{34}S = [(^{34}S/^{32}S)_{sample}/(^{34}S/^{32}S)_{standard}) - 1]$, and given as ‰ values on the VCDT scale via multiplication by 1000. Analytical uncertainty was less than ± 0.05‰, and sample reproducibility was within ± 0.2‰. Sulfide standards used were IAEA-S1, IAEA-S2, IAEA-S3, with values of −0.3, 21.7, and −31.3‰ respectively, on the SO_2 scale.

5. Analytical results

5.1. Zircon U-Pb age

The analytical results of the selected zircon crystals from the Qingmingshan sulfide-bearing mafic intrusion are listed in Table 3. The cathodoluminescence (CL) images of representative zircon crystals and the U-Pb isotope Concordia plot for the selected zircon crystals are illustrated in Fig. 5. A total of 15 spot analyses on 15 selected zircon grains yield a Concordia U-Pb age of 847.8 ± 3.8 Ma (2σ). This age is significantly younger than the maximum depositional age of the sedimentary country rocks (866.7 ± 3.7 Ma, Wang et al., 2007) but significantly older than other dated Neoproterozoic mafic-ultramafic intrusions in the Baotan area (Fig. 2c). The new and old age data together reveal that the Neoproterozoic basaltic magmatism in the area lasted for ~37 myr.

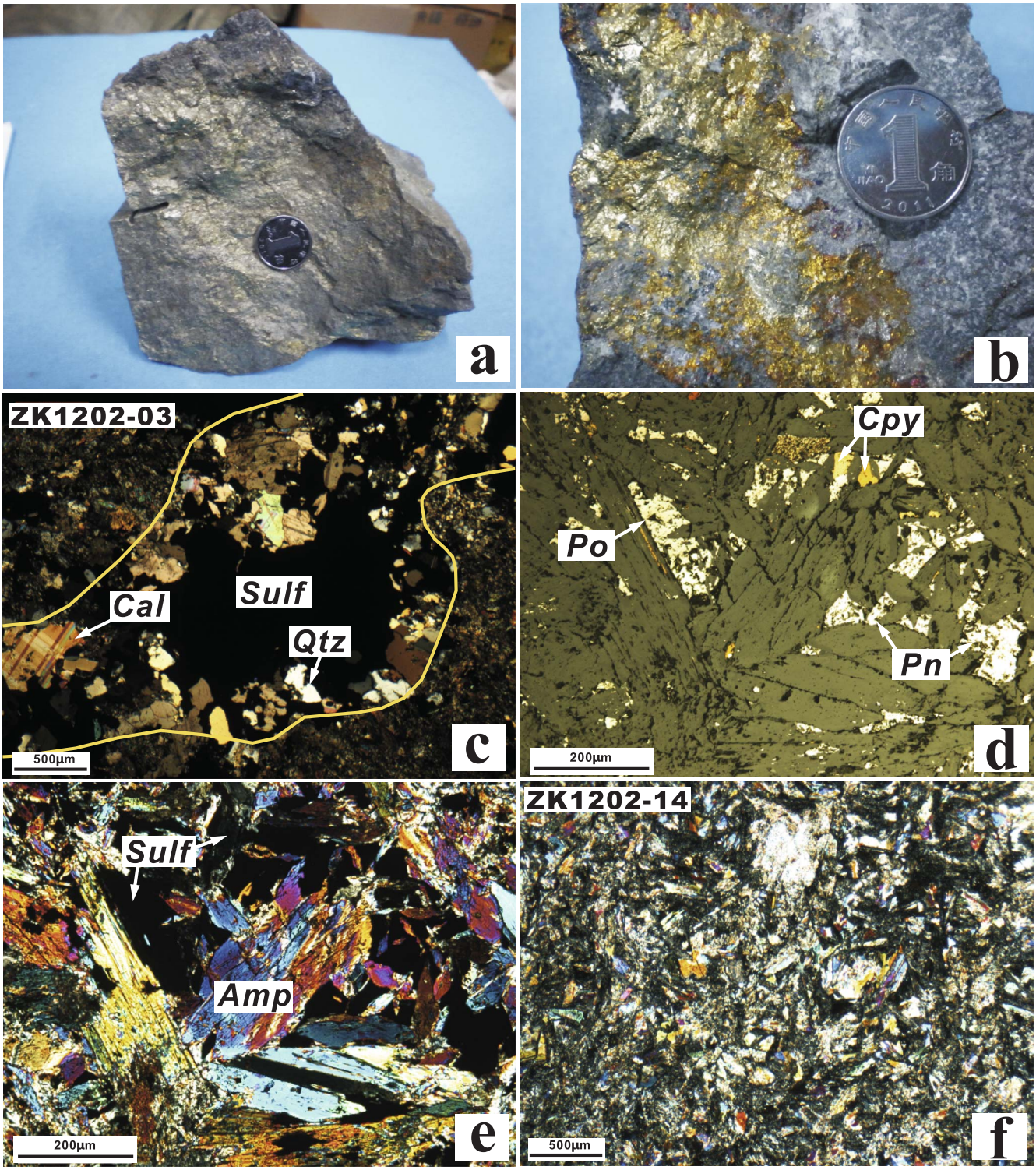

Fig. 4. Photographs of (a) massive sulfide vein and (b) semi-massive sulfide vein, photomicrographs of (c) a sulfide-quartz-calcite intergrowth, (d) disseminated texture, (e) sulfide-bearing meta-gabbronorite, and (f) dolerite. Amp, amphibole; Sulf, sulfide; Po, pyrrhotite; Pn, pentlandite; Cpy, chalcopyrite; Cal, Calcite; Qtz, Quartz.

5.2. Whole-rock major and trace elements

The concentrations of major and trace elements in the Qingmingshan mafic intrusion are listed in Table 4. Because major primary silicate minerals are not preserved in the samples, we used norm compositions for classification. In the norm calculation the raw data were corrected for LOI and sulfide abundances. The latter were estimated from the concentrations of S, Ni and Cu according to the procedure given by Li et al. (2001). The FeO/(FeO + Fe_2O_3) in the samples was assumed to be 0.8, which is 10% lower than the recommended value for basalts but reasonable for mafic-ultramafic cumulate rocks. The results for the samples from drill core ZK1202 are illustrated in Fig. 6a. The stratigraphic variations of whole rock $Mg^{\#}$ [100 × MgO/(MgO + FeO), molar], Cr/V and Ce concentrations are illustrated in Fig. 6b–d. The interval between 372 and 380 m

Table 3
SIMS zircon U-Pb isotopes of the Qingmingshan sulfide-bearing mafic intrusion.

Sample/spot												Apparent age (Ma)					
	U	Th (ppm)	Pb	Th/U	$^{207}Pb/^{206}Pb$	± 1σ (%)	$^{207}Pb/^{235}U$	± 1σ (%)	$^{206}Pb/^{238}U$	± 1σ (%)	ρ	$^{207}Pb/^{206}Pb$	± 1σ	$^{207}Pb/^{235}U$	± 1σ	$^{206}Pb/^{238}U$	± 1σ
ZK30703 (Sulfide-bearing gabbronorite sampled from the drill core ZK30703 of the Qingmingshan deposit in the Baotan area)																	
ZK30703-1	325	202	69	0.62	0.07368	0.67	1.70620	1.64	0.16795	1.50	0.91	1032.8	13.5	1010.9	10.6	1000.8	13.9
ZK30703-3	1639	2049	337	1.25	0.06735	0.41	1.31143	1.57	0.14123	1.51	0.97	848.5	8.5	850.8	9.1	851.6	12.1
ZK30703-4	980	599	695	0.61	0.18657	0.18	13.44695	1.51	0.52272	1.50	0.99	2712.2	3.0	2711.6	14.4	2710.7	33.3
ZK30703-5	2805	5273	675	1.88	0.06716	0.28	1.34896	1.53	0.14569	1.50	0.98	842.6	5.8	867.1	8.9	876.7	12.3
ZK30703-6	132	185	100	1.40	0.16741	0.41	11.13420	1.56	0.48236	1.51	0.96	2532.0	6.9	2534.4	14.6	2537.5	31.7
ZK30703-7	1827	2722	396	1.49	0.06769	0.29	1.32256	1.53	0.14170	1.50	0.98	859.2	5.9	855.6	8.9	854.3	12.0
ZK30703-8	883	1025	174	1.16	0.06697	0.48	1.27710	1.58	0.13831	1.50	0.95	836.8	10.1	835.6	9.0	835.1	11.8
ZK30703-9	2646	5612	660	2.12	0.06715	0.24	1.33515	1.52	0.14421	1.50	0.99	842.4	4.9	861.1	8.9	868.4	12.2
ZK30703-10	916	1032	182	1.13	0.06723	0.40	1.30253	1.56	0.14051	1.50	0.97	845.0	8.3	846.8	9.0	847.5	12.0
ZK30703-12	682	713	129	1.05	0.06703	0.67	1.26354	1.66	0.13672	1.52	0.91	838.7	13.9	829.5	9.5	826.1	11.8
ZK30703-13	1624	2328	344	1.43	0.06705	0.30	1.29186	1.53	0.13973	1.50	0.98	839.4	6.3	842.1	8.8	843.2	11.9
ZK30703-14	1343	1978	291	1.47	0.06743	0.45	1.31374	1.57	0.14131	1.50	0.96	851.0	9.4	851.8	9.1	852.1	12.0
ZK30703-16	2118	2990	447	1.41	0.06769	0.36	1.30098	1.54	0.13939	1.50	0.97	859.1	7.4	846.2	8.9	841.2	11.8
ZK30703-17	2088	3025	446	1.45	0.06706	0.37	1.29438	1.56	0.13999	1.51	0.97	839.6	7.7	843.2	9.0	844.6	12.0
ZK30703-18	2297	3724	518	1.62	0.06699	0.25	1.32639	1.52	0.14361	1.50	0.99	837.3	5.2	857.3	8.9	865.1	12.2
ZK30703-19	2935	4702	628	1.60	0.06717	0.24	1.27502	1.52	0.13767	1.50	0.99	843.1	5.0	834.6	8.7	831.5	11.7
ZK30703-20	2348	4823	577	2.05	0.06750	0.29	1.33763	1.54	0.14372	1.52	0.98	853.3	6.0	862.2	9.0	865.6	12.3
ZK30703-21	1880	2521	397	1.34	0.06762	0.28	1.32215	1.53	0.14182	1.50	0.98	856.8	5.7	855.5	8.9	854.9	12.0

ρ denotes error correlation between $^{207}Pb/^{235}U$ and $^{206}Pb/^{238}U$

(elevation) has very low $Mg^{\#}$. The samples from this interval show a characteristic texture of dolerite (Fig. 4f). Based on these changes we have divided the drill core into three lithological units: a lower zone (LZ, composed of gabbronorites), a middle zone (MZ, composed of a dolerite and a gabbronorite) and an upper zone (UZ, composed of gabbronorites). The sample from the base of the middle unit has high Ce content and low Cr/V, indicating that it is not a cumulate but rather a quenched liquid.

The primitive mantle-normalized immobile incompatible trace element patterns for the Qingmingshan mafic rocks are shown in Fig. 7. The dolerite sample from the base of the middle zone has the highest abundances of the incompatible trace elements. All of the samples from the different parts of the intrusion are characterized by significant enrichments in light rare earth elements (REE) relative to heavy REE and show pronounced negative Nb-Ta anomalies, similar to the characteristics of subalkaline basalts from continental arcs (Li et al., 2015a). In the diagram of $(Th/Nb)_N$ versus $(Th/Yb)_N$, the Qingmingshan mafic rocks all plot between the field for the global Cenozoic continental arc basalts and the average composition of the mudstones of the Sibao Group, the country rocks of the intrusion (Fig. 8). None of the samples plot close to or on the mixing line between OIB and the crustal end-member.

5.3. Re-Os isotopes

The Re-Os isotopic compositions of the Qingmingshan deposit are given in the Table 5. The initial $^{187}Os/^{188}Os$ ratios and $\gamma_{Os}(t)$ values were calculated using the U-Pb age of 847.8 Ma for zircon from the host intrusion. The sulfide-bearing samples analyzed contain 5 to 407 ppb Re and 0.65 to 47 ppb Os_{common}, yielding high Re/Os_{common} ratios ranging from 6 to 18, which are higher than the ratio of the fertile

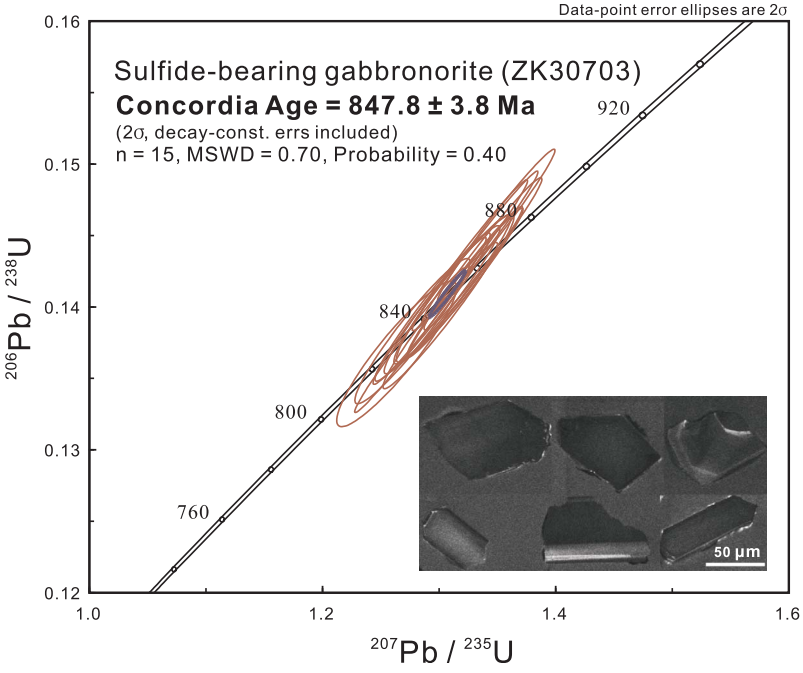

Fig. 5. Zircon U-Pb isotope Concordia diagrams for the Qingmingshan sulfide-bearing mafic intrusion, with representative CL images of selected zircon grains.

Table 4
Whole rock compositions of the Qingmingshan sulfide-bearing mafic intrusion.

Sample	ZK1202-02	ZK1202-03	ZK1202-04	ZK1202-05	ZK1202-06	ZK1202-07	ZK1202-08	ZK1202-09	ZK1202-10	ZK1202-11	ZK1202-12
Location/ Depth(m)	Upper zone of ZK1202										
	357.0	358.6	360.6	362.0	364.0	364.7	367.0	369.2	370.2	372.8	376.5
Rock type	Gn	Gn with vein	Gn	Gn	Gn	Gn	Gn	Gn	Gn	Gn	Gn
SiO_2	43.9	44.6	44.1	45.2	46.0	45.4	44.9	46.2	47.5	46.9	46.4
Al_2O_3	9.94	11.05	9.15	9.46	8.46	8.91	9.51	9.68	9.74	8.94	9.64
Fe_2O_3	15.74	14.80	15.73	13.25	10.78	11.62	12.11	11.16	11.78	11.32	12.44
MgO	15.70	11.40	15.80	17.45	18.85	18.95	17.58	17.32	17.85	18.15	16.80
CaO	6.11	5.82	6.65	6.82	8.54	8.24	7.68	7.53	6.80	8.01	6.95
Na_2O	0.19	1.45	0.70	0.26	0.32	0.35	0.43	0.69	0.55	0.47	0.74
K_2O	0.07	0.80	0.20	0.35	0.09	0.09	0.51	0.55	0.53	0.35	0.59
TiO_2	0.52	0.57	0.41	0.49	0.44	0.46	0.45	0.48	0.49	0.46	0.50
P_2O_5	0.05	0.06	0.04	0.05	0.05	0.04	0.04	0.05	0.05	0.05	0.05
MnO	0.31	0.16	0.20	0.21	0.19	0.19	0.18	0.18	0.18	0.18	0.19
LOI	2.70	0.71	1.84	3.39	3.77	3.48	3.89	4.39	3.54	3.44	3.24
Mg#	75.01	75.42	77.08	77.79	81.23	80.96	79.13	79.35	78.96	79.87	77.84
S (wt%)	1.54	3.29	2.27	0.54	0.06	0.37	0.39	0.12	0.24	0.13	0.36
Ni (ppm)	4636	5470	7229	2357	943	1729	1257	786	1100	1179	1572
Cu (ppm)	2317	12200	3275	959	320	959	1358	320	639	bdl	639
Cs	1.7	2.9	3.5	11.4	2.9	2.6	17.5	19.1	18.6	6.3	19.7
Rb	3.2	39	9.9	27	5.0	5.2	37	41	39	17.3	42
Ba	3.2	168	25	22	7.3	6.7	43	50	47	84	62
Sr	8.4	99	26	14.0	16.7	22	41	47	30	26	34
Pb	29	8.9	96	10.6	31	40	75	43	75	12.8	4.3
Th	2.8	3.1	2.2	2.4	2.8	2.5	2.3	2.8	2.6	2.6	2.6
U	0.62	0.64	0.51	0.55	0.67	0.59	0.50	0.66	0.58	0.63	0.55
Zr	53	61	42	46	56	57	44	50	48	49	48
Hf	1.42	1.60	1.12	1.23	1.50	1.34	1.33	1.39	1.26	1.47	1.33
Ta	0.26	0.23	0.22	0.24	0.25	0.26	0.23	0.26	0.24	0.26	0.27
Y	13.1	14.8	10.6	11.9	12.1	12.8	11.2	12.5	11.6	11.2	12.3
Nb	3.5	3.7	2.7	3.2	3.1	3.1	2.8	3.3	3.1	3.0	3.3
Sc	27	36	26	20	26	28	23	29	18	14	27
Cr	1250	633	1203	1285	1553	1380	1612	1460	1436	1378	1214
Co	184	165	201	96	76	91	129	70	80	75	83
V	177	206	160	164	162	167	171	171	171	153	172
Ga	11.2	11.2	9.0	9.7	8.9	10.2	9.9	9.7	9.7	8.8	9.9
Zn	321	525	210	144	132	163	136	132	141	143	170
La	6.47	8.22	6.19	6.52	5.65	6.26	5.96	8.13	6.72	8.28	7.27
Ce	14.3	17.8	12.5	14.7	13.3	15.3	13.7	17.3	14.7	16.9	15.6
Pr	1.72	2.02	1.47	1.70	1.69	1.93	1.64	2.04	1.80	1.92	1.89
Nd	7.73	7.62	6.42	7.54	7.48	7.98	7.31	8.68	7.79	7.80	7.93
Sm	1.89	1.75	1.55	1.66	1.75	1.83	1.68	1.91	1.82	1.83	1.89
Eu	0.50	0.66	0.45	0.50	0.51	0.56	0.50	0.50	0.50	0.56	0.50
Gd	2.13	2.23	1.72	1.85	1.79	1.82	1.82	2.04	1.96	1.92	1.97
Tb	0.39	0.32	0.30	0.34	0.35	0.37	0.32	0.36	0.36	0.34	0.35
Dy	2.37	2.22	1.89	2.12	2.15	2.10	2.00	2.27	2.16	2.15	2.19
Ho	0.51	0.57	0.39	0.46	0.46	0.47	0.44	0.46	0.47	0.45	0.47
Er	1.48	1.49	1.23	1.37	1.35	1.34	1.31	1.43	1.39	1.33	1.42
Tm	0.21	0.21	0.17	0.20	0.19	0.20	0.19	0.22	0.21	0.19	0.20
Yb	1.35	1.48	1.22	1.30	1.32	1.35	1.27	1.38	1.33	1.32	1.31
Lu	0.19	0.27	0.18	0.19	0.20	0.20	0.18	0.21	0.20	0.20	0.20

Sample	ZK1202-13	ZK1202-14	ZK1202-15	ZK1202-16	ZK1202-17	ZK1202-18	ZK1202-19	ZK1202-20	ZK1202-21
Location/ Depth (m)	Middle zone of ZK1202	Lower zone of ZK1202							
	378.4	380.2	381.2	382.9	384.3	386.5	389.0	390.2	391.5
Rock type	Gn	Dol	Gn	Gn	Gn	Gn	Gn	Gn	Gn
SiO_2	43.6	49.6	46.8	47.2	47.3	46.5	46.3	47.1	47.6
Al_2O_3	9.41	12.60	9.40	9.93	9.84	10.05	10.05	10.15	9.84
Fe_2O_3	17.14	10.67	12.60	11.55	11.60	13.15	13.72	11.74	10.80
MgO	14.10	11.80	17.25	16.40	16.10	15.45	14.90	16.8	17.05
CaO	6.75	5.65	7.18	7.55	7.61	6.7	7.15	7.19	7.16
Na_2O	1.07	3.03	0.53	1.34	1.28	1.3	1.43	1.28	1.04
K_2O	0.85	1.08	0.29	0.27	0.37	0.68	0.64	0.41	0.42
TiO_2	0.49	0.67	0.50	0.52	0.53	0.53	0.54	0.52	0.51
P_2O_5	0.05	0.07	0.05	0.05	0.05	0.06	0.06	0.06	0.05
MnO	0.19	0.15	0.20	0.19	0.19	0.18	0.19	0.2	0.18
LOI	2.09	2.16	4.33	3.93	3.83	3.79	3.66	3.91	4.16
Mg#	75.06	76.12	78.44	79.14	78.55	77.48	77.65	78.00	79.63
S (wt%)	2.96	0.81	0.51	0.50	0.41	1.13	1.65	0.20	0.04
Ni (ppm)	8330	2279	2043	1886	1414	3290	4165	866	550

(continued on next page)

Table 4 *(continued)*

Sample	ZK1202-13	ZK1202-14	ZK1202-15	ZK1202-16	ZK1202-17	ZK1202-18	ZK1202-19	ZK1202-20	ZK1202-21
Location/ Depth (m)	Middle zone of ZK1202	Lower zone of ZK1202							
	378.4	380.2	381.2	382.9	384.3	386.5	389.0	390.2	391.5
Rock type	Gn	Dol	Gn	Gn	Gn	Gn	Gn	Gn	Gn
Cu (ppm)	2956	959	1118	959	639	1900	1917	644	160
Cs	9.0	18.4	9.2	5.6	4.9	10.5	8.4	15.4	11.3
Rb	26	60	21	15.2	18.6	40	33	44	28
Ba	81	318	28	39	68	107	116	87	59
Sr	46	237	22	69	82	125	115	83	63
Pb	23	6.9	21	10.1	11.3	4.1	5.1	4.0	24
Th	2.7	3.8	3.1	2.8	2.7	2.5	3.0	2.5	2.6
U	0.64	0.86	0.70	0.61	0.63	0.55	0.67	0.55	0.57
Zr	53	73	66	52	53	73	56	73	55
Hf	1.40	2.00	1.79	1.49	1.53	1.66	1.49	1.67	1.47
Ta	0.22	0.33	0.26	0.27	0.27	0.23	0.26	0.23	0.26
Y	12.3	18.1	12.5	13.9	13.8	15.6	13.6	14.0	12.7
Nb	3.2	4.7	3.3	3.6	3.6	3.9	3.7	3.6	3.5
Sc	27	34	27	28	29	30	28	30	28
Cr	1430	726	1366	1273	1226	1240	1168	1450	1425
Co	162	111	100	107	88	93	165	57	59
V	174	224	173	184	187	198	187	192	181
Ga	9.7	11.2	10.2	10.0	10.3	12.1	10.2	11.9	10.0
Zn	230	136	195	145	132	127	128	149	151
La	6.83	11.60	7.20	7.75	7.91	7.95	7.99	7.73	7.64
Ce	16.4	23.1	15.6	16.6	16.8	17.5	17.1	16.9	16.6
Pr	1.93	2.66	1.84	1.98	1.94	2.01	2.05	1.92	1.96
Nd	8.29	11.00	7.86	8.39	8.10	7.84	8.67	7.36	8.31
Sm	1.78	2.54	1.76	1.89	1.86	1.81	1.99	1.62	1.97
Eu	0.56	0.65	0.47	0.53	0.55	0.50	0.56	0.47	0.55
Gd	2.00	2.69	1.87	2.11	2.11	2.08	2.05	1.86	1.94
Tb	0.36	0.52	0.35	0.38	0.39	0.35	0.39	0.33	0.37
Dy	2.04	3.14	2.15	2.40	2.35	2.03	2.31	1.88	2.27
Ho	0.50	0.65	0.46	0.51	0.51	0.45	0.48	0.43	0.48
Er	1.34	1.92	1.36	1.48	1.47	1.43	1.54	1.22	1.37
Tm	0.18	0.31	0.20	0.22	0.23	0.19	0.22	0.20	0.20
Yb	1.41	1.84	1.31	1.48	1.45	1.26	1.46	1.13	1.36
Lu	0.22	0.28	0.20	0.20	0.22	0.20	0.20	0.20	0.21

Sample	ZK1202-22	ZK1202-23	ZK30703	LC-1301	LC-1304	LC-1305	LC-1308	LC-1310	LC-1312
Location/ Depth(m)	Lower zone of ZK1202		Drill core	Mining Tunnel					
	393.2	394.2	-	#985	#960	#960	#960	#960	#960
Rock type	Gn	Gn	Gn	Gn	Gn	Massive sulfide vein	Gn	Gn	Gn
SiO_2	47.8	47.1	51.1	48.30	37.3	1.69	35.7	46.4	46.0
Al_2O_3	9.80	9.23	15.30	10.80	8.07	bdl	7.60	9.76	9.59
Fe_2O_3	10.92	11.16	8.49	12.41	25.8	68.50	24.9	13.35	13.66
MgO	17.30	18.50	8.15	14.25	12.35	0.17	12.35	15.75	15.05
CaO	7.01	6.82	11.05	6.05	5.51	0.78	6.16	6.75	6.90
Na_2O	1.00	0.23	1.40	1.41	0.29	bdl	0.29	1.02	0.75
K_2O	0.72	0.82	0.95	1.82	0.25	0.01	0.22	0.99	0.53
TiO_2	0.50	0.47	0.52	0.56	0.42	bdl	0.39	0.51	0.50
P_2O_5	0.05	0.05	0.05	0.06	0.05	0.02	0.05	0.05	0.05
MnO	0.17	0.18	0.15	0.18	0.19	0.03	0.19	0.20	0.22
LOI	4.28	4.36	1.47	3.09	5.71		4.95	3.16	3.64
Mg#	79.69	80.40	70.41	73.97	69.61		69.31	77.71	76.13
S (wt%)	0.06	0.01	0.10	0.11	6.56	34.90	6.78	1.19	1.25
Ni (ppm)	629	471	157	1650	17500	105500	11050	3222	4636
Cu (ppm)	320	80	80	399	5530	810	27400	1997	4154
Cs	25	32	2.0	57	6.0		5.1	18.3	
Rb	52	64	53	164	19.1		17.1	69	
Ba	76	73	134	254	16.9		16.9	210	
Sr	47	12.9	126	82	7.4		8.4	72	
Pb	163	30	8.8	15.7	14.0		14.6	41.1	
Th	2.5	2.9	3.0	2.9	2.2		1.9	2.8	
U	0.57	0.59	0.61	0.63	0.48		0.42	0.65	
Zr	50	66	65	57	41		42	56	
Hf	1.41	1.69	1.82	1.50	1.13		1.05	1.36	
Ta	0.27	0.25	0.24	0.31	0.20		0.17	0.22	
Y	13.4	13.8	14.5	14.0	9.9		9.4	12.6	
Nb	3.6	3.6	3.8	3.9	2.7		2.2	3.4	
Sc	27	29	34	30	24		27	27	
Cr	1471	1700	228	1063	871		905	1250	
Co	86	80	41	77	364		291	115	

(continued on next page)

Table 4 *(continued)*

Sample	ZK1202-22	ZK1202-23	ZK30703	LC-1301	LC-1304	LC-1305	LC-1308	LC-1310	LC-1312
Location/ Depth(m)	Lower zone of ZK1202		Drill core	Mining Tunnel					
	393.2	394.2	-	#985	#960	#960	#960	#960	#960
Rock type	Gn	Gn	Gn	Gn	Gn	Massive sulfide vein	Gn	Gn	Gn
V	178	196	194	198	154		156	175	
Ga	10.0	10.3	14.0	11.6	8.1		7.8	9.9	
Zn	171	234	94	204	204		560	185	
La	9.90	8.38	9.68	7.70	6.33		5.84	8.02	
Ce	18.1	17.4	21.1	17.4	13.6		12.3	17.8	
Pr	2.01	1.86	2.26	2.11	1.46		1.35	1.83	
Nd	8.26	7.78	9.07	9.29	6.35		5.41	7.66	
Sm	1.82	1.76	1.99	2.09	1.55		1.40	1.85	
Eu	0.54	0.54	0.58	0.51	0.40		0.48	0.48	
Gd	2.16	1.85	1.98	2.23	1.34		1.48	1.78	
Tb	0.38	0.35	0.35	0.41	0.28		0.23	0.35	
Dy	2.34	1.99	2.34	2.48	1.77		1.44	2.12	
Ho	0.48	0.45	0.52	0.55	0.38		0.30	0.48	
Er	1.48	1.34	1.44	1.58	1.06		1.08	1.32	
Tm	0.21	0.20	0.22	0.23	0.16		0.18	0.19	
Yb	1.39	1.23	1.44	1.52	0.96		0.88	1.35	
Lu	0.23	0.17	0.22	0.23	0.16		0.16	0.21	

Note: Concentration of FeO in the sulfide has been corrected for samples with S > 0.3wt.% prior to the calculation of Mg#
Mg# = 100 × molar MgO/(MgO + FeO), assuming $FeO_T = 0.8 \times Fe_2O_3$
Major elements are in wt.% and trace elements are in ppm
Abbreviation: Gn = Gabbronorite, Dol = Dolerite, bdl = below detection limit.

mantle (Shirey and Walker, 1998). Sample LC-1301 has the lowest initial $^{187}Os/^{188}Os$ ratio (0.124) and $\gamma_{Os}(t)$ (2.5); these values are similar to those of primitive mantle. The other samples all have elevated initial $^{187}Os/^{188}Os$ and $\gamma_{Os}(t)$ ranging from 0.138 to 0.229 and from 14 to 89, respectively, which are significantly higher than the primitive mantle values.

5.4. Chalcophile elements

The concentrations of S, Cu, Ni and PGE in the sulfide-bearing samples from the Qingmingshan deposit are listed in Table 6. Their stratigraphic variations in drill core ZK1202 are illustrated in Fig. 6e–f. The chalcophile elements vary with depth and show three separate peaks, one in each lithological unit. Each peak corresponds to a disseminated sulfide zone. The samples used in this study are all characterized by Cu/Zr ratios > 1, indicating the presence of cumulus sulfide in the samples (Li and Naldrett, 1999). The Cu/Pd ratios of the samples are all much higher than the mantle value (< 10^4, Barnes and Maier, 1999).

The primitive mantle-normalized chalcophile element patterns for the Qingmingshan deposit are illustrated in Fig. 9. And variations of Ir and Pt tenor as well as Ir and Pd tenor from the Qingmingshan deposit are shown in Fig. 10. A massive sulfide vein (LC-1305, shown in Fig. 4a), a sulfide-quartz-calcite intergrowth (ZK1202-03, shown in Fig. 4c) and the samples containing < 0.36 wt% S are excluded. Metal tenors (i.e., concentrations in recalculated 100% sulfide) are used in the plots. The tenor calculation was done using the equation of Barnes and Lightfoot (2005). The average tenors in disseminated (0.36 wt % < S < 11 wt%) sulfide samples are 12.4 wt% Ni, 5.9 wt% Cu, 66.7 ppb Ir, 86.6 ppb Ru, 26.8 ppb Rh, 1276 ppb Pt, and 454 ppb Pd.

The mantle-normalized chalcophile element patterns for the separate disseminated sulfide zones in the Qingmingshan deposit are similar. They all show depletions in IPGE relative to Ni, depletion in PPGE relative to Cu, and significant fractionation between PPGE and IPGE (Fig. 9). Generally, the PGE tenors and patterns of the Qingmingshan deposit are similar to those of the Nebo-Babel magmatic sulfide deposit that is also hosted in gabbronorites in a Proterozoic orogenic belt in Western Australia (Seat et al., 2009).

5.5. Sulfur isotopes

Sulfur isotope compositions of the Qingmingshan magmatic sulfide deposit are given in Table 7. The $\delta^{34}S$ values vary from 1.8 to 3.2‰, with a peak at 2.6‰ (Fig. 11). No clear difference exists between the different sulfide zones of the deposit. The range of $\delta^{34}S$ values for the Qingmingshan deposit is clearly different from that of the MORB mantle (−1.57 to +0.60‰, Labidi et al., 2013, 2014).

6. Modeling and discussion

6.1. Parent magma composition

Except for a dolerite sample from the base of the middle unit of the host intrusion, all other samples have low incompatible trace element abundances. This, together with the norm compositions (shown in Fig. 6a), suggests that the mafic rocks are pyroxene-plagioclase cumulates. Due to a lack of primary olivine, pyroxenes and plagioclase in the rocks, the Mg/Fe and Ca/Na ratios in the parental magma of these rocks cannot be determined. The best approximation is to use the compositions of the dolerite sample from the base of the middle unit. High incompatible trace element abundances (Fig. 7) and a quenched texture (Fig. 4f) indicate that the compositions of this sample are close to those of a liquid. In other words, the $Mg^{\#}$ and incompatible trace element abundances in this sample may be used to represent the upper and lower limits, respectively. The $Mg^{\#}$ of this sample is estimated to be ~76 (Table 4), which is > 10% lower than that of the average subalkaline basalt from continental arcs (Li et al., 2015a). The average subalkaline basalt from continental arcs is chosen for such a comparison because (1) the Qingmingshan mafic intrusion was emplaced in a continental margin (see Figs. 1 and 2 and associated text), (2) the norm compositions of the Qingmingshan mafic rocks are consistent with the subalkaline magma series and (3) the incompatible trace element patterns of the Qingmingshan mafic rocks match this type of basalt very well (Fig. 7). Based on the difference in whole-rock $Mg^{\#}$ between this sample and the average subalkaline basalt from continental arcs (Li et al., 2015a), the degree of fractional crystallization experienced by the parental magma of the Qingmingshan mafic rocks, estimated using the MELTS program of Ghiorso and Sack (1995), is ~15 wt%. A high degree of olivine fractionation for the parental magma of the

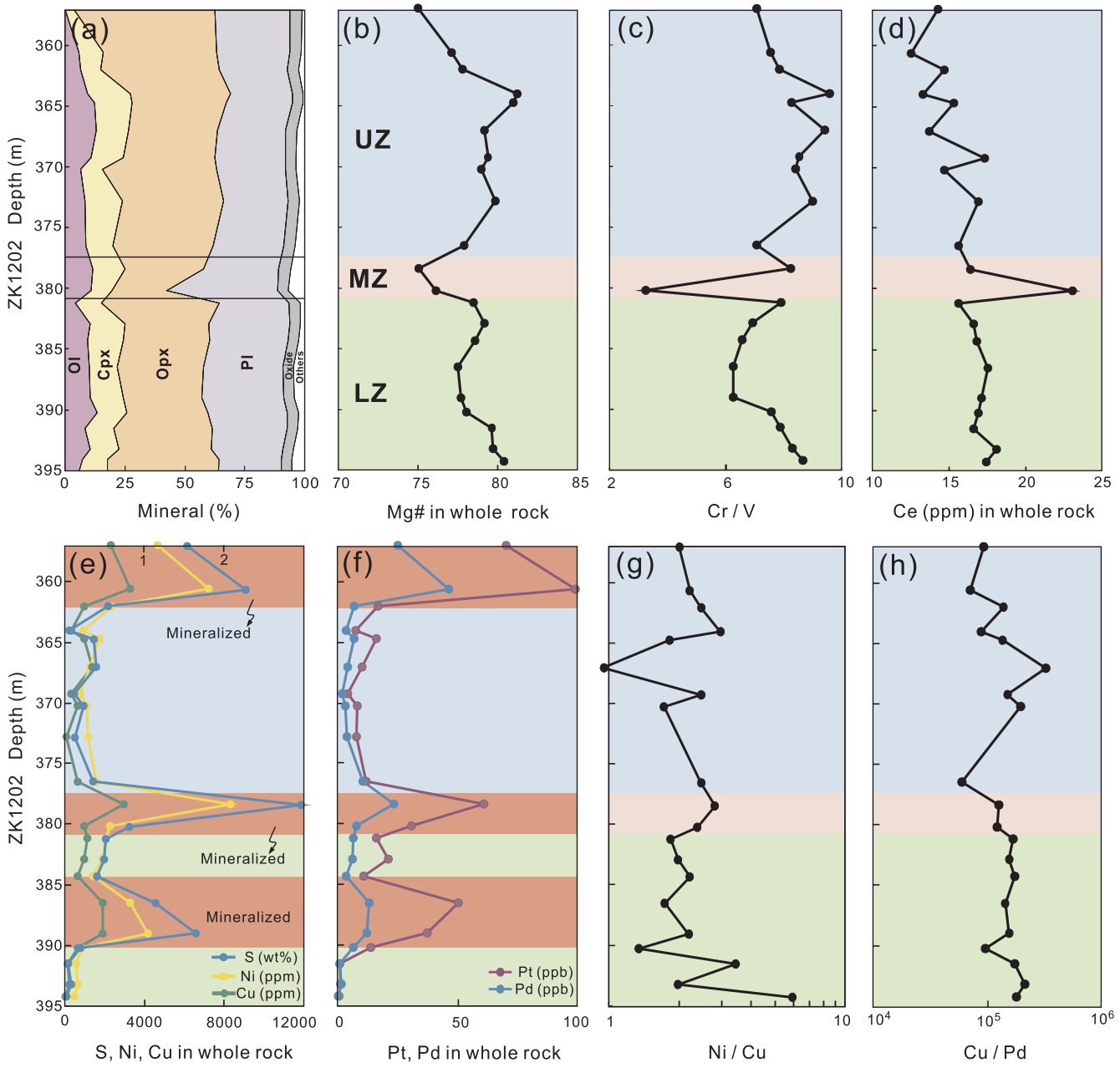

Fig. 6. Stratigraphic variations of (a) major rock-forming mineral abundances (in wt%), (b) Mg# of whole rocks, (c) Cr/V of whole rocks, (d) Ce concentration in whole rocks, (e) S, Cu, Ni contents in whole rocks, (f) Pt and Pd contents in whole rocks, (g) Ni/Cu of whole rocks and (h) Cu/Pd of whole rocks. LZ, lower zone; MZ, middle zone; UZ, upper zone.

Qingmingshan magmatic sulfide deposit is also indicated by its low Ni/Cu ratios. The average Ni/Cu value of the Qingmingshan deposit is ~2, which is within the range of Ni/Cu values (1–4) of several magmatic sulfide deposits in Eastern Tianshan, such as Huangshandong, Huangshanxi and Heishan (Fig. 12) that formed from moderately fractionated magma in convergent tectonic settings (Song et al., 2016; Xie et al., 2014). The average Ni/Cu value of the Qingmingshan deposit is about 3 times lower than the Ni/Cu ratios of the Xiarihamu deposit (4–15) that formed from primitive arc basalt (Li et al., 2015c; Song et al., 2016).

6.2. Crustal contamination and sulfide saturation

The addition of S and Os from continental crust to the parental magma of the Qingmingshan deposit is indicated by elevated $\delta^{34}S$ (Fig. 11) and $\gamma_{Os}(t)$ values (Table 5) for the sulfides. Sr-Nd isotopes are good indicators for contamination with siliceous crustal materials. In the absence of these isotope data, we have tried to use trace element ratios such as $(Th/Nb)_N$ and $(Th/Yb)_N$ as an alternative. As shown in Fig. 8, the variations of $(Th/Nb)_N$ and $(Th/Yb)_N$ in the Qingmingshan mafic intrusion is consistent with mixing between continental arc basalt and the mudstones of the Sibao Group (the country rocks of the intrusion). The degrees of crustal contamination in the parental magma are estimated to be 10–20 wt% (Fig. 8). Our mixing calculation shows that OIB is not the right choice for the mantle-derived magma that generated the Qingmingshan mafic intrusion, because the mafic rocks all plot far away from the mixing line between this magma and the contaminant.

The forgoing analysis indicates that both siliceous contamination and addition of crustal S and Os took place during the evolution of the Qingmingshan magmatic system. We cannot determine which one is more important in triggering sulfide saturation in the magma based on the data we have.

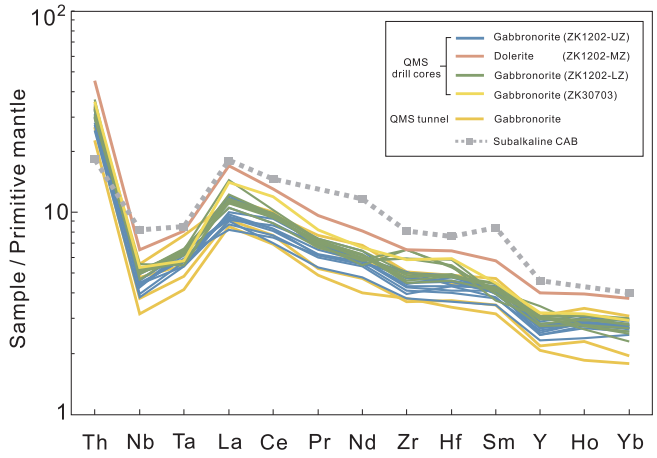

Fig. 7. Primitive mantle-normalized immobile incompatible element patterns for the Qingmingshan sulfide-bearing mafic intrusion. The normalization values are from Palme and O'Neill (2014). The average composition of subalkaline-CAB is from Li et al. (2015a). Abbreviations are the same as in Fig. 6.

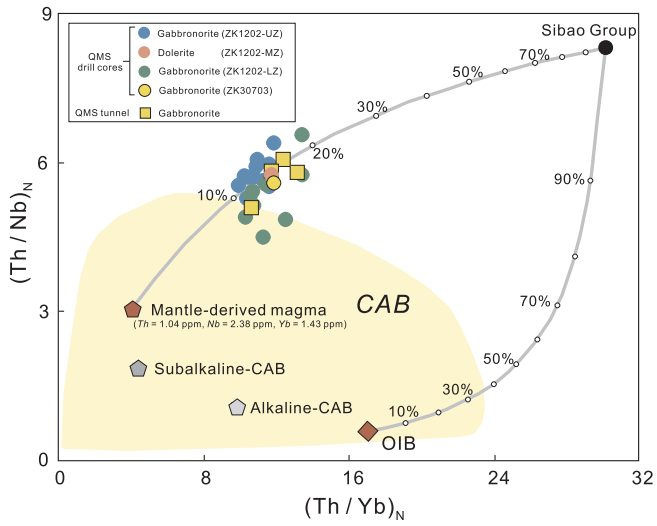

Fig. 8. Plot of mantle-normalized $(Th/Nb)_N$ vs. $(Th/Yb)_N$ for the Qingmingshan sulfide-bearing mafic intrusion. The compositions of continental arc basalts (CAB) are from GEOROC (http://georoc.mpch-mainz.gwdg.de/georoc/). The average compositions of ocean island basalts (OIB), subalkaline-CAB and alkaline-CAB are from Li et al. (2015a). The composition of the Sibao Group is the average compositions of 22 mudstone samples from the Sibao Group (Wang et al., 2012). Mantle-derived magma compositions are assumed to be 1.04 ppm Th, 2.38 ppm Nb, 1.43 ppm Yb. The normalization values are from Palme and O'Neill (2014). Abbreviations are the same as in Fig. 6.

6.3. Controls on PGE tenors

There are three major controls on the concentrations of PGE in immiscible sulfide liquids: (1) the initial contents of PGE in the parental magma; (2) the R factor (magma/sulfide mass ratio, Campbell and Naldrett, 1979) during sulfide segregation; (3) fractional crystallization of monosulfide solid solution from sulfide liquid upon cooling (e.g., Li et al., 1992). The last process commonly does not have significant effect on the PGE tenor variations of disseminated sulfide samples because it is difficult for sulfide liquid to escape from such rocks during sulfide liquid fractional crystallization. Metal tenors in a sulfide liquid are controlled by both their initial concentrations in the magma and R-factor. Hence, a useful estimation for the initial concentration of a metal in the magma requires a well-constrained R-factor. Since the contents of Cu in basalts are far more restricted than PGE, Cu is a good choice for setting the lower limit for R-factors. Based on average Cu content in basalts, some researchers (e.g., Naldrett, 2011; Barnes and Lightfoot, 2005) have shown that a minimum R-factor close to 300 is required to produce a sulfide liquid containing > 3 wt% Cu. Since the average Cu tenor of the Qingmingshan deposit is close to 3 wt%, we will use a R-factor of 300 as the lower limit in our estimation of initial PGE concentrations in the parental magma of the Qingmingshan deposit. Based on the partition coefficients of $D_{Ir} = 5 \times 10^4$, $D_{Pt} = 4 \times 10^4$ and $D_{Pd} = 3 \times 10^4$ between sulfide melt and silicate magma (Mungall and Brenan, 2014), the initial concentrations of Ir, Pt and Pd in the parent magma of the Qingmingshan deposit are estimated to be 0.11 ppb, 1.89 ppb Pt and 0.72 ppb respectively (Fig. 10), which are about one order of magnitude lower than the values of PGE-undepleted picrites associated with the Siberian flood basalts (Lightfoot and Keays, 2005) but similar to the values in the parental magmas of all known subduction-related magmatic sulfide deposits in China such as Heishan (Xie et al., 2014) and Xiarihamu (Zhang et al., 2017). Variations of PGE tenors in different sulfide zones can be explained by R-factors ranging from 300 to 1000 during sulfide segregation from the magma (Fig. 10).

6.4. A conceptual model and exploration implications

Despite their similar ages, the Jinchuan and Qingmingshan magmatic sulfide deposits are inferred to occur in different tectonic settings. The former is related to rift-related magmatism in a continental margin (Li and Ripley, 2011) whereas the latter is related to arc magmatism based on the results from this study. Given the geometry, internal structure and lithogeochemical variation in the Qingmingshan sulfide-bearing mafic intrusion, it is reasonable to propose that this intrusion was a feeder to arc basaltic volcanism. It is suggested that at least three separate pulses of magma went through the plumbing system, each of them carried tiny sulfide droplets (Fig. 13). Most of the sulfide droplets, together with pyroxene crystals were trapped in the Qingmingshan dike while the magma continued to ascend.

Based on the results of this study the Qingmingshan deposit is different from the Jinchuan deposit, including the formation age and the tectonic setting of the magmatism. For these reasons exploration for Jinchuan-type deposits in this region are not warranted. However, as indicated by the recent discovery of the Xiarihamu deposit, arc-type mafic-ultramafic intrusions can also host major magmatic sulfide deposits (Li et al., 2015c).

It is suggested that sulfide saturation in the Qingmingshan magmatic system took place at depth (Fig. 13). Thus, at the deposit scale, exploration at greater depth makes sense. At a general scale, coeval mafic-ultramafic intrusions that formed from more primitive magma (i.e., containing more primitive olivine) are more promising, because these intrusions have potential to host sulfide ores that have higher Ni/Cu ratios and hence are more valuable than the Qingmingshan deposit.

7. Conclusions

Zircon U-Pb isotope data show that the Qingmingshan sulfide-bearing mafic intrusions formed at 847.8 ± 3.8 Ma, and are ~37 myr older than the youngest mafic-ultramafic intrusions in the Baotan area. The protracted nature of basaltic magmatism in such a small area reinforces the notion that the Neoproterozoic mafic-ultramafic intrusions in this area are the products of arc basaltic magmatism. This interpretation is also supported by the arc-like mantle-normalized incompatible trace element characteristics of the Qingmingshan intrusive rocks, such as light REE enrichments relative to heavy REE and pronounced negative Nb-Ta anomalies. Whole rock major element compositions indicate that except a dolerite, other rocks in the intrusion are pyroxene-plagioclase cumulates of a basaltic magma that underwent strong olivine fractionation (~15 wt% fractional crystallization). PGE tenors of the Qingmingshan magmatic sulfide deposit are very low, indicating a severely PGE-depleted parental magma. S-Os isotopes indicate that crustal S and Os are present in the Qingmingshan magmatic

Table 5
Re-Os isotopic compositions of samples from the Qingmingshan deposit.

Sample	Location	Sulfide texture	Re (ppb)	Os_{common}	Re/Os_{common}	$^{187}Re/^{188}Os$	± 1σ	$^{187}Os/^{188}Os$	± 1σ	$(^{187}Os/^{188}Os)_i$	γOs(t)
LC-1301	Mining tunnel	Weakly disseminated	11.93	0.650	18.37	88.88	0.90	1.3886	0.0038	0.1243	2.48
LC-1304	Mining tunnel	Disseminated	66.90	6.989	9.57	46.36	0.47	0.8155	0.0012	0.1560	28.6
LC-1308	Mining tunnel	Disseminated	73.40	7.277	10.09	48.59	0.49	0.8305	0.0012	0.1394	14.9
LC-1308	Duplicate analysis		72.89	7.387	9.87	47.76	0.48	0.8212	0.0012	0.1418	16.9
LC-1312	Mining tunnel	Disseminated	20.40	2.139	9.54	46.03	0.46	0.8131	0.0012	0.1583	30.5
ZK1202-02	Drill core (UZ)	Disseminated	31.00	3.312	9.36	45.17	0.46	0.7875	0.0044	0.1450	19.6
ZK1202-07	Drill core (UZ)	Weakly disseminated	6.43	1.033	6.22	30.02	0.30	0.5974	0.0009	0.1704	40.5
ZK1202-11	Drill core (UZ)	Weakly disseminated	5.10	0.676	7.54	36.42	0.37	0.6561	0.0014	0.1381	13.9
ZK1202-13	Drill core (MZ)	Disseminated	49.98	6.562	7.62	36.93	0.37	0.6815	0.0010	0.1562	28.7
ZK1202-16	Drill core (LZ)	Weakly disseminated	8.66	1.203	7.20	34.74	0.35	0.6355	0.0010	0.1413	16.5
ZK1202-19	Drill core (LZ)	Disseminated	22.43	2.655	8.45	40.63	0.48	0.7228	0.0011	0.1449	19.4
P-1*		Massive	388	46.80	8.29	39.2	0.4	0.734	0.009	0.1764	45.4
P-11*		Massive	407	36.21	11.24	53.2	0.5	0.986	0.012	0.2293	89.0

Note: $\lambda = 1.666 \times 10^{-11}$/year, t = 847.8 Ma; the primitive initial $^{187}Os/^{188}Os$, $(^{187}Os/^{188}Os)_i$, is assumed to be 0.09531, and the average $^{187}Re/^{188}Os$ of chondrites is 0.40186 (after Shirey and Walker, 1998).
Abbreviation: UZ = Upper zone, MZ = Middle zone, LZ = Lower zone
* Source data come from Mao and Du, 2002. Common Os concentrations are calculated from data therein. Their initial $^{187}Os/^{188}Os$ ratios and γOs values are recalculated using t = 847.8 Ma.

Table 6
Concentrations of S, Ni, Cu and PGE in the Qingmingshan deposit.

Sample	Location (Depth/m)	Zone	Sulfide texture	S	Ni	Cu	Ir	Ru	Rh	Pt	Pd
				(wt%)	(ppm)		(ppb)				
ZK1202-02	Drill core ZK1202 (357)	UZ	Disseminated	1.54	4636	2317	2.95	3.66	1.54	70.24	25.20
ZK1202-04	Drill core ZK1202 (360.6)	UZ	Disseminated	2.27	7229	3275	5.08	6.12	2.02	98.98	46.20
ZK1202-05	Drill core ZK1202 (362)	UZ	Weakly disseminated	0.54	2357	959	1.06	1.39	0.43	16.98	6.89
ZK1202-06	Drill core ZK1202 (364)	UZ	Weakly disseminated	0.06	943	320	0.44	0.66	0.23	7.70	3.62
ZK1202-07	Drill core ZK1202 (364.7)	UZ	Weakly disseminated	0.37	1729	959	1.01	1.19	0.29	16.28	7.06
ZK1202-08	Drill core ZK1202 (367)	UZ	Weakly disseminated	0.39	1257	1358	bdl	0.84	0.28	10.15	4.14
ZK1202-09	Drill core ZK1202 (369.2)	UZ	Weakly disseminated	0.12	786	320	0.27	0.36	0.13	4.28	2.13
ZK1202-10	Drill core ZK1202 (370.2)	UZ	Weakly disseminated	0.24	1100	639	0.56	0.68	0.21	8.24	3.23
ZK1202-11	Drill core ZK1202 (372.8)	UZ	Weakly disseminated	0.13	1179	bdl	0.76	0.93	0.27	7.82	3.97
ZK1202-12	Drill core ZK1202 (376.5)	UZ	Weakly disseminated	0.36	1572	639	0.71	1.02	0.31	11.72	10.65
ZK1202-13	Drill core ZK1202 (378.4)	MZ	Disseminated	2.96	8330	2956	bdl	5.63	1.84	61.08	23.58
ZK1202-14	Drill core ZK1202 (380.2)	MZ	Weakly disseminated	0.81	2279	959	1.65	2.09	0.76	30.80	7.96
ZK1202-15	Drill core ZK1202 (381.2)	LZ	Weakly disseminated	0.51	2043	1118	1.09	1.32	0.39	16.31	6.62
ZK1202-16	Drill core ZK1202 (382.9)	LZ	Weakly disseminated	0.50	1886	959	1.00	1.54	0.41	21.00	6.14
ZK1202-17	Drill core ZK1202 (384.3)	LZ	Weakly disseminated	0.41	1414	639	0.57	0.73	0.23	10.79	3.62
ZK1202-18	Drill core ZK1202 (386.5)	LZ	Disseminated	1.13	3290	1900	1.76	2.49	0.63	50.22	13.27
ZK1202-19	Drill core ZK1202 (389)	LZ	Disseminated	1.65	4165	1917	1.96	2.98	0.95	37.34	12.30
ZK1202-20	Drill core ZK1202 (390.2)	LZ	Weakly disseminated	0.20	866	644	0.39	0.39	0.12	14.02	6.71
ZK1202-21	Drill core ZK1202 (391.5)	LZ	Weakly disseminated	0.04	550	160	0.07	0.10	0.04	1.09	0.91
ZK1202-22	Drill core ZK1202 (393.2)	LZ	Weakly disseminated	0.06	629	320	0.17	0.25	0.08	1.38	1.49
ZK1202-23	Drill core ZK1202 (394.2)	LZ	Weakly disseminated	0.01	471	80	0.04	0.05	0.02	0.65	0.44
LC-1301	Mining tunnel		Weakly disseminated	0.11	1650	399	0.47	0.78	0.32	10.46	3.84
LC-1304	Mining tunnel		Disseminated	6.56	17500	5530	6.88	8.28	2.55	100.26	36.73
LC-1305	Mining tunnel		Massive	34.90	105500	810	63.30	100.93	28.10	37.55	64.20

Abbreviations: UZ = Upper zone; MZ = Middle zone; LZ= Lower zone; bdl = below detection limit.

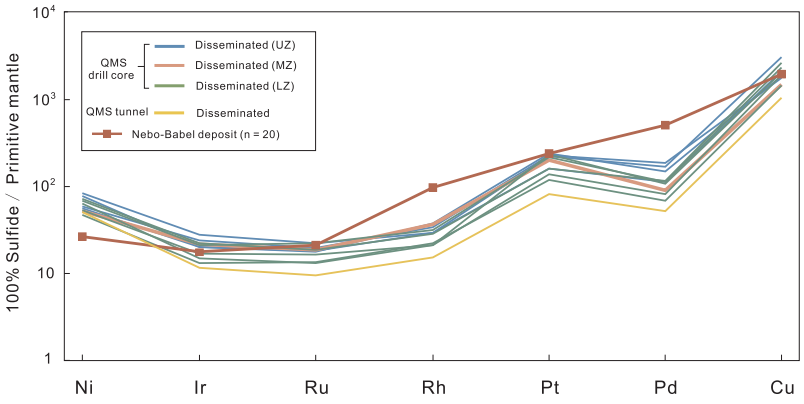

Fig. 9. Primitive mantle-normalized patterns of metal tenors for the Qingmingshan sulfide deposit. The disseminated sulfide samples with S > 0.36 wt% are used. The average metal tenors in sulfide ores of the Nebo-Babel deposit are from Seat et al. (2009). The normalization values are from Barnes and Lightfoot (2005). Abbreviations are the same as in Fig. 6.

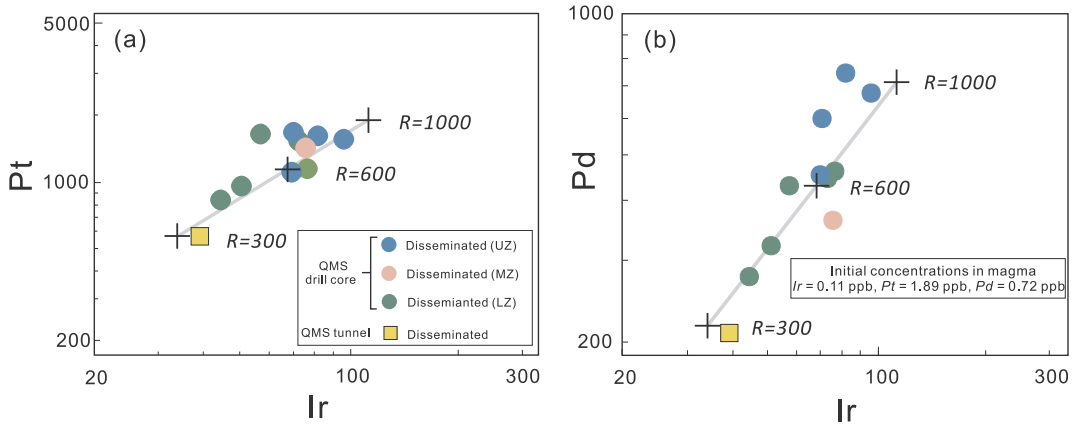

Fig. 10. (a) Plot of Ir tenor vs. Pt tenor and (b) Plot of Ir tenor vs. Pd tenor for the Qingmingshan magmatic sulfide deposit. The disseminated sulfide samples with S > 0.36 wt% are used. Abbreviations are the same as in Fig. 6.

Table 7
S isotopes of samples from the Qingmingshan deposit.

Sample	Location	Host Rock	Sulfide texture	Sulfide mineral assemblage	$\delta^{34}S$
LC-1304	Mining tunnel	Gabbronorite	Disseminated	*Po + Cp + Pn*	2.35
LC-1305	Mining tunnel	Gabbronorite	Massive	*Po + Cp + Pn*	2.72
LC-1308	Mining tunnel	Gabbronorite	Disseminated	*Po + Cp + Pn*	2.06
ZK1202-02	Drill core (UZ)	Gabbronorite	Disseminated	*Po + Cp + Pn*	1.82
ZK1202-02	*Duplicate analysis*				2.04
ZK1202-07	Drill core (UZ)	Gabbronorite	Weakly disseminated	*Po + Cp + Pn*	2.83
ZK1202-10	Drill core (UZ)	Gabbronorite	Weakly disseminated	*Po + Cp + Pn*	2.99
ZK1202-13	Drill core (MZ)	Gabbronorite	Disseminated	*Po + Cp + Pn*	2.44
ZK1202-14	Drill core (MZ)	Dolerite	Weakly disseminated	*Po + Cp + Pn*	2.52
ZK1202-15	Drill core (LZ)	Gabbronorite	Weakly disseminated	*Po + Cp + Pn*	3.03
ZK1202-17	Drill core (LZ)	Gabbronorite	Weakly disseminated	*Po + Cp + Pn*	3.15
ZK1202-19	Drill core (LZ)	Gabbronorite	Disseminated	*Po + Cp + Pn*	2.73
ZK1202-21	Drill core (LZ)	Gabbronorite	Weakly disseminated	*Po + Cp + Pn*	2.67

Abbreviations: UZ = Upper zone, MZ = Middle zone, LZ = Lower zone, Po = Pyrrhotite, Cp = Chalcopyrite, Pn = Pentlandite.
$\delta^{34}S$ values are in per mil (‰), relative to V-CDT.

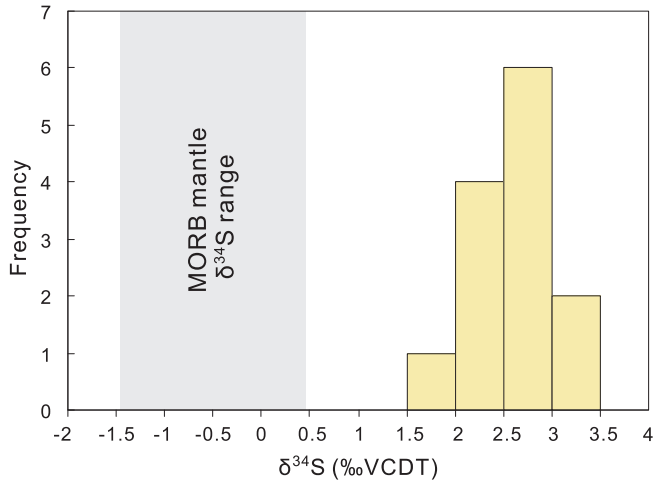

Fig. 11. Histogram of $\delta^{34}S$ values of sulfide separates from the Qingmingshan magmatic sulfide deposit. The range of $\delta^{34}S$ for mid-ocean ridge basalts (MORB) is from Labidi et al. (2013, 2014).

sulfides. Siliceous contamination is indicated by $(Th/Nb)_N$ and $(Th/Yb)_N$ in whole rocks. It is suggested that the Qingmingshan magmatic sulfide deposit formed in a dynamic conduit through which at least three separate pulses of sulfide-charged magma passed through. The deeper part of the system is a favorable exploration target. It is recommended that exploration for magmatic sulfide deposits with higher Ni tenors than the Qingmingshan deposit focus on the Neoproterozoic ultramafic intrusions that formed from more primitive arc magmas in the region.

Acknowledgments

This study was jointly supported by the National Natural Science Foundation of China (41425011) and the Strategic Priority Research Program (B) of the Chinese Academy of Sciences (XDB18030000). The manuscript was completed during the first author's visit to Indiana University, funded by the Institute of Geochemistry, Chinese Academy of Sciences. The authors thank Jing Hu, Yi-fan Yin and Yan Huang for their assistance with trace elements and PGE measurements at the SKLODG. Li-min Zhou are thanked for the Re-Os isotope analysis, and Benjamin Underwood for help with sulfur isotope analyses. Dr. Wen-jun Hu and Dr. Si-qi Yang are thanked for their assistance with the SIMS zircon U-Pb analyses and field work, respectively. Many discussions between Benjamin Wernette and the first author are greatly appreciated. We acknowledge the Jishengyuan Mining Ltd for access to the mine and permission to collect samples. Qingfu Meng from this mining corporation is gratefully thanked for assistance in field work and providing relevant mining data. Constructive comments from the reviewer and guest editors, and editorial guidance from the editor-in-chief are greatly appreciated.

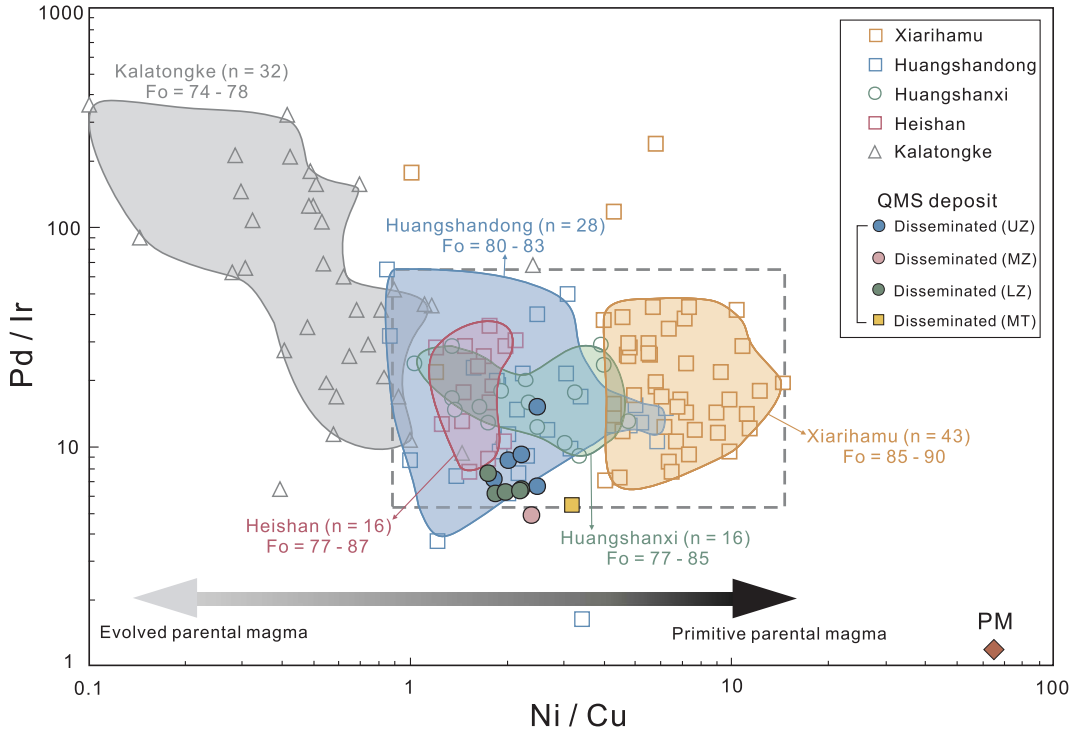

Fig. 12. Plot of Ni/Cu vs. Pd/Ir of disseminated sulfide samples (S contents from 0.36 to 11 wt%) from some magmatic sulfide deposits in convergent tectonic settings in China. Data sources: Xiarihamu (Li et al., 2015c; Song et al., 2016; Zhang et al., 2017), Huangshandong (Deng et al., 2012, 2014; Mao et al., 2015; Sun et al., 2013), Huangshanxi (Zhang et al., 2011; Mao et al., 2014), Heishan (Xie et al., 2014), Kalatongke (Gao et al., 2012; Li et al., 2012; Song and Li, 2009). MT = Mining tunnel. PM = Primitive mantle (data from Barnes and Lightfoot, 2005). Other abbreviations are the same as in Fig. 6.

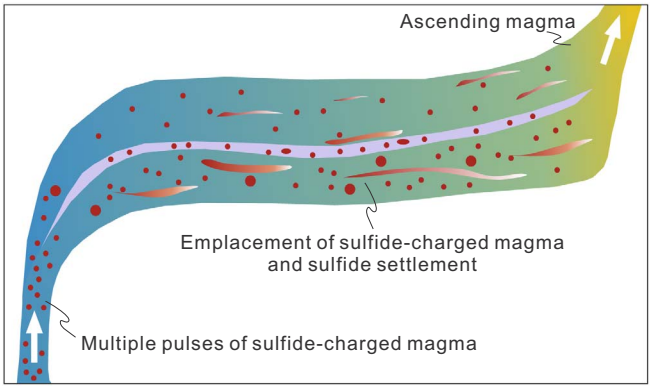

Fig. 13. A conceptual model (not to scale) for the Qingmingshan ore-forming system. See text for details.

References

Barnes, S.J., Lightfoot, P.C., 2005. Formation of magmatic nickel sulfide ore deposits and processes affecting their copper and platinum group element contents. Econ. Geol. 100th anniversary volume 34, 179–214.

Barnes, S.J., Maier, W., 1999. The fractionation of Ni, Cu and the noble metals in silicate and sulphide liquids. Dynamic processes in magmatic ore deposits and their application to mineral exploration. Geological Association of Canada, Short Course Notes 13, 69–106.

BGMRGX (Bureau of Geology and Mineral Resources of Guangxi province), 1985. Regional Geology of Guangxi Autonomous Region. Geological Publishing House, Beijing, pp. 1–853 (in Chinese with English Abstract).

BGMRGZ (Bureau of Geology and Mineral Resources of Guizhou Province), 1987. Regional Geology of Guizhou Province. Geological Publishing House, Beijing, pp. 1–698 (in Chinese with English abstract).

Campbell, I.H., Naldrett, A.J., 1979. The influence of silicate:sulfide ratios on the geochemistry of magmatic sulfides. Econ. Geol. 74, 1503–1506.

Charvet, J., 2013. The Neoproterozoic-Early Paleozoic tectonic evolution of the South China Block: an overview. J. Asian Earth Sci. 74, 198–209.

Chen, X., Wang, D., Wang, X.L., Gao, J.F., Shu, X.J., Zhou, J.C., 2014. Neoproterozoic chromite-bearing high-Mg diorites in the western part of the Jiangnan orogen, southern China: geochemistry, petrogenesis and tectonic implications. Lithos 200, 35–48.

Deng, Y.F., Song, X.Y., Zhou, T.F., Yuan, F., Chen, L.M., Zheng, W.Q., 2012. Correlations between Fo number and Ni content of olivine of the Huangshandong intrusion, eastern Tianshan, Xinjiang and the genetic significances. Acta Petrol. Sinica 28, 2224–2234 (in Chinese with English abstract).

Deng, Y.-F., Song, X.-Y., Chen, L.-M., Zhou, T., Pirajno, F., Yuan, F., Xie, W., Zhang, D., 2014. Geochemistry of the Huangshandong Ni–Cu deposit in northwestern China: implications for the formation of magmatic sulfide mineralization in orogenic belts. Ore Geol. Rev. 56, 181–198.

Gao, J.F., Zhou, M.F., Lightfoot, P.C., Wang, C.Y., Liang, Q.I., 2012. Origin of PGE-poor and Cu-rich magmatic sulfides from the Kalatongke deposit, Xinjiang, Northwest China. Econ. Geol. 107, 481–506.

Ge, W.C., Li, X.H., Li, Z.X., Zhou, H.W., 2001. Mafic intrusions in Longsheng area: age and its geological implications. Chin. J. Geol. 36, 112–118 (in Chinese with English abstract).

Ghiorso, M.S., Sack, R.O., 1995. Chemical mass transfer in magmatic processes IV. A revised and internally consistent thermodynamic model for the interpolation and extrapolation of liquid–solid equilibria in magmatic systems at elevated temperatures and pressures. Contrib. Mineral. Petrol. 119, 197–212.

GXRGST (Guangxi Regional Geological Survey Team), 1964. Regional Geological Survey Report (Xing'an area, 1:200,000) (in Chinese).

GXRGST (Guangxi Regional Geological Survey Team), 1966. Regional Geological Survey Report (Sanjiang area, 1:200,000) (in Chinese).

GXRGST (Guangxi Regional Geological Survey Team), 1987. Regional Geological Survey Report (Baotan area, 1:50,000) (in Chinese).

GXRGST (Guangxi Regional Geological Survey Team), 1995. Regional Geological Survey Report (Sanfang area, 1:50,000) (in Chinese).

GZRGST (Guizhou Regional Geological Survey Team), 1974. Regional Geological Survey Report of Fanjingshan area (1:50,000) (in Chinese).

Han, C., Xiao, W., Su, B., Sakyi, P.A., Ao, S., Zhang, J., Wan, B., Song, D.F., Wang, Z.M., 2016. Ages and tectonic implications of the mafic–ultramafic-carbonatite intrusive rocks and associated Cu-Ni, Fe-P and apatite-vermiculite deposits from the Quruqtagh district, NW China. Ore Geol. Rev. http://dx.doi.org/10.1016/j.oregeorev.2016.07.011.

Labidi, J., Cartigny, P., Moreira, M., 2013. Non-chondritic sulphur isotope composition of the terrestrial mantle. Nature 501, 208–211.

Labidi, J., Cartigny, P., Hamelin, C., Moreira, M., Dosso, L., 2014. Sulfur isotope budget (32S, 33S, 34S and 36S) in Pacific-Antarctic ridge basalts: A record of mantle source heterogeneity and hydrothermal sulfide assimilation. Geochim. Cosmochim. Acta 133, 47–67.

Li, X.H., 1999. U-Pb zircon ages of granites from the southern margin of the Yangtze Block: timing of Neoproterozoic Jinning: Orogeny in SE China and implications for Rodinia Assembly. Precambr. Res. 97, 43–57.

Li, C., Naldrett, A.J., 1999. Geology and petrology of the Voisey's Bay intrusion: reaction

of olivine with sulfide and silicate liquids. Lithos 47, 1–31.
Li, C., Ripley, E.M., 2011. The giant Jinchuan Ni-Cu-(PGE) deposit: tectonic setting, magma evolution, ore genesis and exploration implications. Rev. Econ. Geol. 17, 163–180.
Li, C., Naldrett, A.J., Coats, C., Johannessen, P., 1992. Platinum, palladium, gold, copper-rich stringers at the Strathcona Mine, Sudbury; their enrichment by fractionation of a sulfide liquid. Econ. Geol. 87, 1584–1598.
Li, Z.X., Li, X.H., Kinny, P.D., Wang, J., 1999. The breakup of Rodinia: did it start with a mantle plume beneath South China? Earth Planet. Sci. Lett. 173, 171–181.
Li, C., Maier, W.D., De Waal, S., 2001. Magmatic Ni-Cu versus PGE deposits: contrasting genetic controls and exploration implications. S. Afr. J. Geol. 104, 309–318.
Li, Z.X., Li, X.H., Zhou, H.W., Kinny, P.D., 2002. Grenvillian continental collision in south China: new SHRIMP U-Pb zircon results and implications for the configuration of Rodinia. Geology 30, 163–166.
Li, X.H., Su, L., Chung, S.L., Li, Z., Liu, Y., Song, B., Liu, D., 2005. Formation of the Jinchuan ultramafic intrusion and the world's third largest Ni–Cu sulfide deposit: associated with the 825 Ma south China mantle plume? Geochem. Geophys. Geosyst. 6. http://dx.doi.org/10.1029/2005GC001006.
Li, X.H., Liu, Y., Li, Q.L., Guo, C.H., Chamberlain, K.R., 2009. Precise determination of Phanerozoic zircon Pb/Pb age by multicollector SIMS without external standardization. Geochem. Geophys. Geosyst. 10, Q04010. http://dx.doi.org/10.1029/2009GC002400.
Li, C., Zhang, M., Fu, P., Qian, Z., Hu, P., Ripley, E.M., 2012. The Kalatongke magmatic Ni–Cu deposits in the Central Asian Orogenic Belt, NW China: product of slab window magmatism? Miner. Deposita 47, 51–67.
Li, C., Arndt, N.T., Tang, Q., Ripley, E.M., 2015a. Trace element indiscrimination diagrams. Lithos 232, 76–83.
Li, C., Yang, X., Zhao, H., Zhou, L.M., Du, A.D., Li, X.W., Qu, W.J., 2015b. High precise isotopic measurements of pg-ng Os by negative ion thermal ionization mass spectrometry. Rock. Miner. Anal. 34, 392–398 (in Chinese with English abstract).
Li, C., Zhang, Z., Li, W., Wang, Y., Sun, T., Ripley, E.M., 2015c. Geochronology, petrology and Hf–S isotope geochemistry of the newly-discovered Xiarihamu magmatic Ni–Cu sulfide deposit in the Qinghai-Tibet plateau, western China. Lithos 216–217, 224–240.
Lightfoot, P.C., Keays, R.R., 2005. Siderophile and chalcophile metal variations in flood basalts from the Siberian trap, Noril'sk region: implications for the origin of the Ni-Cu-PGE sulfide ores. Econ. Geol. 100, 439–462.
Lin, M., Peng, S., Jiang, X., Polat, A., Kusky, T., Wang, Q., Deng, H., 2016. Geochemistry, petrogenesis and tectonic setting of Neoproterozoic mafic–ultramafic rocks from the western Jiangnan orogen, South China. Gondwana Res. 35, 338–356.
Liu, J.S., Yang, Z.J., Dou, S., Yin, L.J., Kang, Y.L., Yang, L.G., 2010. Analysis of Geologic and geochemical characteristic and potential of Cu-Ni sulfide deposits associated with overflow basalt: a case study of the Qingmingshan Cu-Ni sulfide deposit, Guangxi Province. Geol. Explorat. 46, 687–697 (in Chinese with English Abstract).
Ludwig, K.R., 2012. User's Manual for Isoplot 3.75: A Geochronological Toolkit for Microsoft Excel. Berkeley Geochronological Center, Ludwing Special Publication No. 5.
Mao, J.W., Du, A.D., 2002. The 982 Ma Re-Os age of copper-nickel sulfide ores in the Baotan area, Guangxi and its geological significance. Sci. China Ser. D 45, 911–920.
Mao, Y.J., Qin, K.Z., Li, C., Xue, S.C., Ripley, E.M., 2014. Petrogenesis and ore genesis of the Permian Huangshanxi sulfide ore-bearing mafic-ultramafic intrusion in the Central Asian Orogenic Belt, western China. Lithos 200–201, 111–125.
Mao, Y.J., Qin, K.Z., Li, C., Tang, D.M., 2015. A modified genetic model for the Huangshandong magmatic sulfide deposit in the Central Asian Orogenic Belt, Xinjiang, western China. Miner. Deposita 50, 65–82.
Mungall, J.E., Brenan, J.M., 2014. Partitioning of platinum-group elements and Au between sulfide liquid and basalt and the origins of mantle-crust fractionation of the chalcophile elements. Geochim. Cosmochim. Acta 125, 265–289.
Munteanu, M., Wilson, A.H., Yao, Y., Chunnett, G., Luo, Y., 2010. Sequence of magma emplacement and sulfide saturation in the Gaojiacun-Lengshuiqing intrusive complex (SW China). Miner. Deposita 45, 517–529.
Naldrett, A.J., 2011. Fundamentals of magmatic sulfide deposits. Rev. Econ. Geol. 17, 1–50.
Palme, H., O'Neill, H.S.C., 2014. Cosmochemical estimates of mantle composition. In: Richard, W.C. (Ed.), Treatise on Geochemistry, second ed. Elsevier, Amsterdam, pp. 1–39.
Qi, L., Hu, J., Gregoire, D.C., 2000. Determination of trace elements in granites by inductively coupled plasma mass spectrometry. Talanta 51, 507–513.
Qi, L., Gao, J.F., Huang, X.W., Hu, J., Zhou, M.F., Zhong, H., 2011. An improved digestion technique for determination of platinum group elements in geological samples. J. Anal. Atom. Spectrom. 26, 1900–1904.
Seat, Z., Beresford, S.W., Grguric, B.A., Gee, M.M., Grassineau, N.V., 2009. Reevaluation of the role of external sulfur addition in the genesis of Ni-Cu-PGE deposits: evidence from the Nebo-Babel Ni-Cu-PGE deposit, West Musgrave, Western Australia. Econ. Geol. 104, 521–538.
Shirey, S.B., Walker, R.J., 1998. The Re-Os isotope system in cosmochemistry and high-temperature geochemistry. Annu. Rev. Earth Planet. Sci. 26, 423–500.
Shu, L., 2012. An analysis of principal features of tectonic evolution in South China Block. Geol. Bull. China 31, 1035–1053.
Song, X.Y., Li, X.R., 2009. Geochemistry of the Kalatongke Ni–Cu–(PGE) sulfide deposit, NW China: implications for the formation of magmatic sulfide mineralization in a postcollisional environment. Miner. Deposita 44, 303–327.
Song, X.Y., Yi, J.N., Chen, L.M., She, Y.W., Liu, C.Z., Dang, X.Y., Yang, Q.A., Wu, S.K., 2016. The Giant Xiarihamu Ni-Co Sulfide Deposit in the East Kunlun Orogenic Belt, Northern Tibet Plateau, China. Econ. Geol. 111, 29–55.
Studley, S., Ripley, E.M., Elswick, E., Dorais, M., Fong, J., Finkelstein, D., 2002. Analysis of sulfides in whole rock matrices by elemental analyzer–continuous flow isotope ratio mass spectrometry. Chem. Geol. 192, 141–148.
Sun, T., Qian, Z.Z., Deng, Y.F., Li, C., Song, X.Y., Tang, Q.Y., 2013. PGE and isotope (Hf-Sr-Nd-Pb) constraints on the origin of the Huangshandong magmatic Ni-Cu sulfide deposit in the Central Asian Orogenic Belt, Northwestern China. Econ. Geol. 108, 1849–1864.
Wang, J., Li, Z.X., 2003. History of Neoproterozoic rift basins in South China: implications for Rodinia break-up. Precambr. Res. 122, 141–158.
Wang, X.L., Zhou, J.C., Qiu, J.S., Zhang, W.L., Liu, X.M., Zhang, G.L., 2006. LA-ICP-MS U-Pb zircon geochronology of the Neoproterozoic igneous rocks from Northern Guangxi, South China: implications for tectonic evolution. Precambr. Res. 145, 111–130.
Wang, X.C., Li, X.H., Li, W.X., Li, Z.X., 2007. Ca. 825 Ma komatiitic basalts in South China: First evidence for > 1500 degrees C mantle melts by a Rodinian mantle plume. Geology 35, 1103–1106.
Wang, X.L., Zhou, J.C., Griffin, W., Wang, R.C., Qiu, J.S., O'Reilly, S., 2007. Detrital zircon geochronology of Precambrian basement sequences in the Jiangnan orogen: dating the assembly of the Yangtze and Cathaysia Blocks. Precambr. Res. 159, 117–131.
Wang, X.L., Zhou, J.C., Qiu, J.S., Jiang, S.Y., Shi, Y.R., 2008. Geochronology and geochemistry of Neoproterozoic mafic rocks from western Hunan, South China: implications for petrogenesis and post-orogenic extension. Geol. Mag. 145, 215–233.
Wang, W., Zhou, M.F., Yan, D.P., Li, J.W., 2012. Depositional age, provenance, and tectonic setting of the Neoproterozoic Sibao Group, southeastern Yangtze Block, South China. Precambr. Res. 192, 107–124.
Wang, X.L., Zhou, J.C., Griffin, W.L., Zhao, G., Yu, J.H., Qiu, J.S., 2014. Geochemical zonation across a Neoproterozoic orogenic belt: Isotopic evidence from granitoids and metasedimentary rocks of the Jiangnan orogen, China. Precambr. Res. 242, 154–171.
Xie, W., Song, X.Y., Chen, L.M., Deng, Y.F., Zheng, W.Q., Wang, Y.S., Ba, D.H., Yin, M.H., Luan, Y., 2014. Geochemistry insights on the genesis of the subduction-related Heishan magmatic Ni-Cu-(PGE) Deposit, Gansu, Northwestern China, at the Southern Margin of the Central Asian Orogenic Belt. Econ. Geol. 109, 1563–1583.
Yang, Z.J., Liu, J.S., Yin, L.J., Dong, S., Yang, L.G., Kang, Y.L., 2010a. Analysis on the ore-forming mechanism and potential of Cu-Ni sulfide deposits in Baotan Area, Guibei Region, China. Acta Mineral. Sinica 30, 379–388 (in Chinese with English Abstract).
Yang, Z.J., Liu, J.S., Ouyang, Y.F., Yin, L.J., 2010b. Geochemical characteristics and the metallogenic analysis of Qingmingshan basic-ultrabasic intrusion. Contrib. Geol. Miner. Resourc. Res. 25, 141–146 (in Chinese with English Abstract).
Yao, J.L., Shu, L.S., Santosh, M., Zhao, G., 2014. Neoproterozoic arc-related mafic–ultramafic rocks and syn-collision granite from the western segment of the Jiangnan Orogen, South China: constraints on the Neoproterozoic assembly of the Yangtze and Cathaysia Blocks. Precambr. Res. 243, 39–62.
Zhang, M., Kamo, S.L., Li, C., Hu, P., Ripley, E.M., 2010. Precise U-Pb zircon–baddeleyite age of the Jinchuan sulfide ore-bearing ultramafic intrusion, western China. Miner. Deposita 45, 3–9.
Zhang, M., Li, C., Fu, P., Hu, P., Ripley, E.M., 2011. The Permian Huangshanxi Cu–Ni deposit in western China: intrusive–extrusive association, ore genesis, and exploration implications. Miner. Deposita 46, 153–170.
Zhang, Y., Wang, Y., Fan, W., Zhang, A., Ma, L., 2012. Geochronological and geochemical constraints on the metasomatised source for the Neoproterozoic (~825 Ma) high-mg volcanic rocks from the Cangshuipu area (Hunan Province) along the Jiangnan domain and their tectonic implications. Precambr. Res. 220–221, 139–157.
Zhang, Z., Tang, Q., Li, C., Wang, Y., Ripley, E.M., 2017. Sr-Nd-Os-S isotope and PGE geochemistry of the Xiarihamu magmatic sulfide deposit in the Qinghai-Tibet plateau, China. Miner. Deposita 52, 51–68.
Zhao, G., 2015. Jiangnan Orogen in South China: developing from divergent double subduction. Gondwana Res. 27, 1173–1180.
Zhao, G., Cawood, P.A., 1999. Tectonothermal evolution of the Mayuan Assemblage in the Cathaysia Block; implications for Neoproterozoic collision-related assembly of the South China Craton. Am. J. Sci. 299, 309–339.
Zhao, G., Cawood, P.A., 2012. Precambrian geology of China. Precambr. Res. 222–223, 13–54.
Zhao, J.H., Zhou, M.F., 2013. Neoproterozoic high-Mg basalts formed by melting of ambient mantle in South China. Precambr. Res. 233, 193–205.
Zhao, J.H., Zhou, M.F., Yan, D.P., Zheng, J.P., Li, J.W., 2011. Reappraisal of the ages of Neoproterozoic strata in South China: no connection with the Grenvillian orogeny. Geology 39, 299–302.
Zhou, M.F., Yan, D.P., Kennedy, A.K., Li, Y.Q., Ding, J., 2002. SHRIMP U-Pb zircon geochronological and geochemical evidence for Neoproterozoic arc-magmatism along the western margin of the Yangtze Block, South China. Earth Planet Sci. Lett. 196, 51–67.
Zhou, J.C., Wang, X.L., Qiu, J.S., Gao, J.F., 2004. Geochemistry of Meso- and neoproterozoic mafic-ultramafic rocks from northern Guangxi, China: arc or plume magmatism? Geochem. J. 38, 139–152.
Zhou, J.B., Li, X.H., Ge, W., Li, Z.X., 2007. Age and origin of middle Neoproterozoic mafic magmatism in southern Yangtze Block and relevance to the break-up of Rodinia. Gondwana Res. 12, 184–197.
Zhou, J.C., Wang, X.L., Qiu, J.S., 2009. Geochronology of Neoproterozoic mafic rocks and sandstones from northeastern Guizhou, South China: coeval arc magmatism and sedimentation. Precambr. Res. 170, 27–42.